AFOSR-TR-97-0665

REPORT DOCUMENTATION PAGE

Public reporting burden for this collection of information is estimated to average 1 hour per response, including the time for reviewing instructions, searching existing data sources, gathering and maintaining the data needed, and completing and reviewing the collection of information. Send comments regarding this burden estimate or any other aspect of this collection of information, including suggestions for reducing this burden, to Washington Headquarters Services, Directorate for Information Operations and Reports, 1215 Jefferson Davis Highway, Suite 1204, Arlington, VA 22202-4302, and to the Office of Management and Budget, Paperwork Reduction Project (0704-0188), Washington, DC 20503.

1. AGENCY USE ONLY (*Leave Blank*)	2. REPORT DATE October 30, 1997	3. REPORT TYPE AND DATES COVERED Final Report 6/1/94 - 07/31/97

4. TITLE AND SUBTITLE

Synthesis and Characterization of Mechanically Alloyed Ordered Intermetallic Materials.

5. FUNDING NUMBERS

Grant AFOSR

F49620-94-1-0233

6. AUTHORS

Dr. Marek Dollar - Principal Investigator   Dr. Philip Nash - Co-Principal Investigator
Dr. Stan Dymek - Senior Research Associate   Dr. Soon-Chul Ur - Research Assistant
Mr. Hahn Choo - Research Assistant   Mr. Keith Leonard - Research Assistant

7. PERFORMING ORGANIZATION NAME(S) AND ADDRESS(ES)
Illinois Institute of Technology
Mechanical, Materials and Aerospace Engineering Department
Chicago, Il. 60616

8. PERFORMING ORGANIZATION REPORT NUMBER

5-54720

9. SPONSORING / MONITORING AGENCY NAME(S) AND ADDRESS(ES)
Department of the Air Force
Air Force Office of Scientific Research
Bolling Air Force Base, DC 20332-6448

NA

10. SPONSORING / MONITORING AGENCY REPORT NUMBER

11. SUPPLEMENTARY NOTES

12a. DISTRIBUTION / AVAILABILITY STATEMENT

Unlimited   Approved for public release;
distribution unlimited.

12b. DISTRIBUTION CODE

13. ABSTRACT (*Maximum 200 words*)

This report summarizes our studies aimed at improving high temperature strength and creep resistance of mechanically alloyed (MA) intermetallics. MA and hot extruded NiAl was subjected to normal grain growth and secondary recrystallization (SRx) and the latter mechanism proved to significantly improve creep resistance. The minimum creep rate in SRx material was decreased one to two orders of magnitude in comparison to creep in the as-extruded condition. A different approach was to first synthesize NiAl powder containing AlN dispersion and then to fabricate composites containing Al2O3 fibers. The composite processed in the present study is one of the strongest NiAl-based alloys ever produced. In yet another attempt to optimize high temperature properties of intermetallics more refractory, Nb3Al - based materials were produced. It has been shown that mechanical alloying followed by hot pressing is a viable processing route for niobium aluminide intermetallics. The compressive strength of the examined materials was found to be superior to that in the NiAl, but the ductility was lower. The minimum creep rates were found to be approximately one order of magnitude less than those in MA NiAl. The creep rates in the present materials approach those in NASAIR 100, a first generation Ni-base single crystal superalloy.

14. SUBJECT TERMS

Mechanical Alloying, Ordered Intermetallics, Creep, Composites

15. NUMBER OF PAGES

16. PRICE CODE

17. SECURITY CLASSIFICATION OF REPORT Unclassified	18. SECURITY CLASSIFICATION OF THIS PAGE Unclassified	19. SECURITY CLASSIFICATION OF ABSTRACT Unclassified	20. LIMITATION OF ABSTRACT Unlimited UL

ILLINOIS INSTITUTE OF TECHNOLOGY

Mechanical, Materials and Aerospace Engineering Department
Chicago Illinois 60616

FINAL REPORT

SYNTHESIS AND CHARACTERIZATION OF MECHANICALLY ALLOYED ORDERED INTERMETALLIC MATERIALS

Prepared for

by

Marek Dollar	Principal Investigator
Philip Nash	Co-principal Investigator
Stanislaw Dymek	Senior Research Associate
Soon-Chul Ur	Research Assistant
Hahn Choo	Research Assistant
Keith Leonard	Research Assistant

October 1997

EXECUTIVE SUMMARY

Mechanical alloying (MA) of powders followed by hot pressing or extrusion has been used in our laboratory to produce NiAl-based materials. As reported earlier, the technique proved to be capable of producing fully dense, free of cracks, fine grained materials containing a bimodal distribution of aluminum oxide dispersoids. The mechanically alloyed (MA) materials produced in our laboratory were much stronger at both ambient and elevated temperatures and significantly more ductile than their cast counterparts. Minimum creep rates in the MA NiAl were on average three orders of magnitude lower than those in their cast counterparts. The creep resistance of the MA NiAl was found to be better than that of solid solution- and other dispersion-strengthened NiAl and comparable to the creep resistance of precipitation-strengthened NiAl.

This report summarizes our recent attempts to further improve high temperature strength and creep resistance of MA intermetallics.

The first approach was to subject MA NiAl to normal grain growth and secondary recrystallization (SRx) and the latter mechanism proved to significantly improve creep resistance. The minimum creep rate in SRx material was decreased one to two orders of magnitude in comparison to creep in the as-extruded condition. This indicates a contribution from grain boundary sliding to the creep rate of these materials.

A different approach was to first synthesize NiAl powder containing about 5% AlN dispersion by mechanical alloying of elemental nickel and aluminum under a nitrogen gas atmosphere. Then, composites containing 5, 15 and 30 vol.% of Al_2O_3 fibers in addition to the AlN dispersion particles were fabricated by hot pressing a dry blend of the MA NiAl powder and the fibers. As-fabricated microstructures revealed that the composite is fully dense and bonded well with the randomly distributed Al_2O_3 fibers. Neither chemical reaction nor cracks were observed at the fiber/matrix interface. The current composite is one of the strongest NiAl-based alloys ever produced.

In yet another attempt to optimize high temperature properties of intermetallics we focused on a more refractory, Nb_3Al compound. The materials based on Nb_3Al offer a potential for high temperature structural applications because of this compound's high melting point and moderate density. It has been shown that mechanical alloying followed by hot pressing is a viable processing route for niobium aluminide intermetallics. The compressive strength of the examined materials was found to be superior to the NiAl alloy processed and tested at the same conditions, but the ductility was lower. The minimum creep rates of both tested materials were found to be approximately one order of magnitude less than those in MA NiAl.

The creep rates in the present materials approach those in NASAIR 100, a first generation Ni-base single crystal superalloy.

TABLE OF CONTENTS

PART A : NiAl-BASED MATERIALS

A STUDY OF NORMAL GRAIN GROWTH, SECONDARY RECRYSTALLIZATION, AND HIGH TEMPERATURE PROPERTIES IN MECHANICALLY ALLOYED NiAl

PART B : NiAl-BASED FIBER-REINFORCED COMPOSITES

1300K COMPRESSIVE BEHAVIOR OF NiAl-AlN-Al$_2$O$_3$ COMPOSITES

PART C : Nb$_3$Al-BASED MATERIALS

SYNTHESIS AND CHARACTERIZATION OF MECHANICALLY ALLOYED INTERMETALLIC Nb$_3$Al-BASE ALLOYS

PART A : NiAl-BASED MATERIALS

A STUDY OF NORMAL GRAIN GROWTH, SECONDARY RECRYSTALLIZATION, AND HIGH TEMPERATURE PROPERTIES IN MECHANICALLY ALLOYED NiAl

Mechanical alloying of powders followed by hot extrusion has been used in our laboratory to produce NiAl-based materials. As we reported earlier, the technique proved to be capable of producing fully dense, free of cracks, fine grained materials containing a bimodal distribution of aluminum oxide dispersoids. The mechanically alloyed (MA) materials produced in our laboratory were much stronger at both ambient and elevated temperatures and significantly more ductile than their cast counterparts. Minimum creep rates in the MA NiAl were on average three orders of magnitude lower than that in their cast counterparts. The creep resistance of the MA NiAl was found to be better than that of solid solution- and other dispersion-strengthened NiAl and comparable to the creep resistance of precipitation-strengthened NiAl. We demonstrated that improved mechanical properties of the present materials result from their unique microstructure.

In yet another attempt to further improve creep resistance of MA NiAl, the material was subjected to normal grain growth and secondary recrystallization and the latter mechanism proved to significantly improve creep resistance. Actually, the density compensated creep rate of secondary recrystallized MA NiAl is comparable to some superalloys, as can be seen in Fig. 12. What follows is a report on the results of our studies on the modifications of the microstructure of MA NiAl and their effects on mechanical properties. The results of our TEM studies on crept MA NiAl specimens were described in the 1995 first progress report.

1. INTRODUCTION

Improvements in the creep resistance of dispersion strengthened (DS) materials are known to result from an increase in grain size and grain aspect ratio [1,2]. Furthermore, the creep rate was shown to be proportional to the dispersoid size [2,3]. Consequently, the production of coarse grain structures, in combination with a fine dispersoid size represents an attractive design philosophy to improve the creep properties in mechanically alloyed (MA) NiAl. To achieve this, secondary recrystallization (SRx) must be used, since SRx represents a mechanism that can give a pronounced increase in grain size, without concurrent dispersoid coarsening, in a clear contrast to normal grain growth (NGG).

In our laboratory, a study was undertaken to determine the conditions for SRx to occur and then to produce a coarse grain structure by SRx which can be induced by thermomechanical treatment of MA NiAl. The normal grain growth behavior in MA NiAl, which is frequently observed during simple isothermal annealing, was also characterized [4]. The results of these studies can be summarized as follows:

-       Grain growth was observed in the consolidated MA NiAl on isothermal annealing in excess of 1325°C. Abrupt grain growth occurred around 1375°C corresponding to

enhanced dispersoid coarsening. The grain growth obeys the normal grain growth equation of the form $D=kt^n$. The time exponent was about 0.3 and increased with increasing temperature as is typical of DS materials. The apparent activation energy for grain growth was found to be 162 kJ/mole. This appears to be higher than the activation energy for normal grain growth in single phase NiAl, indicating that typical controlling mechanism by boundary diffusion in normal grain growth was affected by dispersoid interactions.

- The dispersoid coarsening accompanying grain growth also obeys the normal type of particle coarsening kinetics of the form $L=kt^n$, where L is dispersoid spacing. The mean particle spacing increases with increasing temperature and the time exponent is less than 1/4 which is less than that of conventional Ostwald ripening theory, assuming that particle coarsening is controlled by grain boundary diffusion. The activation energy for dispersoid coarsening was found to be 143 kJ/mole which is on the order of the activation energy for grain boundary diffusion of Ni in NiAl. The particle coarsening involves the drag of dispersoids by migration of grain boundaries during normal grain growth, leading to particle encounters and coalescence.

- Inhibition of normal grain growth and the presence of texture were shown to be prerequisites for secondary recrystallization to occur. SRx can be developed in these materials during isothermal annealing under certain processing conditions which provide residual strain energy and/or result in finer grain size. The occurrence of SRx was shown to be enhanced by providing an additional driving force in the form of strain energy of cold work. Grain boundary movement during SRx was shown to be very rapid and the grain boundaries bypassed the dispersoids resulting in a much finer dispersoid size in the SRx region than in the normal grain growth region.

- Large, elongated grains having a grain aspect ratio of 5 were produced by SRx after the thermomechanical treatments. The secondary recrystallization temperature (T_{SRx}) depends on extrusion parameters and amount of prestrain. The <110> texture in the as extruded MA NiAl is strengthened after SRx.

In this report, we present the results of our recent studies on the effects of the grain coarsening mechanisms (SRx and NGG) on mechanical properties at ambient and high temperatures. Creep properties of grain coarsened MA NiAl are compared with those of as-consolidated MA NiAl and correlated with the microstructures. The mechanisms controlling creep and the threshold stress behavior in SRx MA NiAl are also explored.

2. EFFECT OF GRAIN COARSENING ON MECHANICAL PROPERTIES

In order to investigate the effect of grain coarsening on mechanical properties, specimens were isothermally annealed at 1375°C for one hour for normal grain growth and SRx specimens

were prepared by thermomechanical treatment including 5% prestrain at room temperature and subsequent annealing at 1300°C for one hour. The unrecrystallized regions at the ends of specimens were removed during EDM machining. The grain size in normal grain growth specimens was about 7 μm and that in SRx specimens about 2000 μm in the transverse section with each grain running the full 8mm length of the specimen.

2.1. Microhardness Measurements

Based on results of isothermal annealing experiments, microstructures with different grain sizes and dispersoid spacings were produced. Microhardness (HV) was measured and an attempt to correlate it with grain size (D) and dispersoid spacing (L) was made. The data were plotted as shown in Fig. 1. A linear regression analysis based on the data gives;

$$HV = -129.7 + 215.6D^{-\frac{1}{2}} + 804.6L^{-\frac{1}{2}}$$

Thus, a Hall-Petch type relationship between the microhardness and both grain size and dispersoid spacing was found in the present study. Also, the microhardness is affected stronger by dispersoid spacing than by grain size in MA NiAl.

HV measurements were performed on sections parallel and perpendicular to the extrusion axis in both NGG and SRxed material to determine if there was an orientation dependence of the mechanical properties. No distinguishable differences in both directions were found.

2.2. Hot Compression Tests

Flow curves (true stress-strain curves) of SRxed MA NiAl at 800°C, 850°C and 900°C are presented in Fig. 2. The flow curve of NGG material tested at 800°C, which was produced by isothermal annealing at 1375°C for an hour, is also presented in Fig. 3. The 0.2% offset yield stresses and total strains are listed in Table 1.

Table 1. Yield Stress and Strain of SRx and NGG MA NiAl

Specimen	Temperature	Yield Stress Mpa	Strain
NGG	800°C	181	0.28*
SRx	800°C	224	0.28*
SRx	850°C	192	0.28*
SRx	900°C	160	0.28*

* Strains at which tests were stopped.

The general trend in high temperature flow behavior of the specimens grain coarsened by either NGG or SRx is shown to be similar to that of as-extruded specimens [5], exhibiting continuous yielding followed by work softening. Work softening behavior was frequently

observed in dispersion strengthened NiAl during hot compression tests above 800 K, presumably due to either microcrack formation or dynamic recovery during the hot deformation process [6]. Though microcrack formation might be considered responsible for the work softening due to the compression test mode [6], the inherent work softening mechanism by dynamic recovery or dynamic recrystallization [7] is believed to be responsible in this case. Although microcracks were occasionally found in the hot compression test specimens, most specimens which did not form microcracks during the test also showed work softening behavior. Recent TEM studies support the hypothesis since specimens deformed at high temperature exhibited much lower dislocation density than those deformed at lower temperature after the same amount of deformation [8].

As expected, the coarser microstructure in the NGG and SRx specimens leads to lower yield stresses below 800°C in comparison with as-extruded specimens, Fig. 4. The higher yield stress in SRx specimens, compared to NGG specimens, at 800°C, is believed to result from the finer dispersoid size in the SRx specimens. The 0.2% offset yield stress of the SRx specimens exceeds that of the as-extruded specimens at 900°C, indicating that grain boundary sliding makes a significant contribution to the strain at that temperature and strain rate of 8.5×10^{-4} sec^{-1}. This result is in agreement with that reported in MA NiAl-Fe, where flow stress at a strain rate of 2×10^{-4} sec^{-1} is very sensitive to grain size at 1000°C [9]. Grain size strengthening is generally expected during low temperature deformation, where slip by dislocation glide is dominant [10,11], but flow stress is expected to be directly proportional to grain size once diffusional deformation conditions are predominant, usually at high temperature and low stress.

3. CREEP PROPERTIES OF GRAIN COARSENED MA NIAL

3.1. General Creep Trends

Compressive creep tests were performed on SRxed and NGG specimens, at a constant load applied parallel to the extrusion axis ranging from 40 MPa to 180MPa at 800°C, 850°C and 900°C for 20 hours. The normalized creep condition in this study is $0.56 \leq T/T_M \leq 0.61$ and $4 \times 10^{-4} \leq \sigma/G \leq 3 \times 10^{-3}$, assuming no significant differences in shear modulus between as-extruded and SRx conditions. Creep curves of grain coarsened specimens obtained at 850°C and 110 MPa are presented in Fig. 5. In the figure, creep curves of as consolidated MA NiAl as well as cast NiAl are presented for comparison. The creep curves show primary and steady state creep but not tertiary creep, due to the compressive creep mode used in which most microstructural instabilities such as microcracking or necking are suppressed [6].

As can be seen, the creep resistance of MA NiAl is considerably improved by SRx, while the curve of NGG specimen shows very poor creep resistance despite a larger grain size compared to as-consolidated specimens. Significant dispersoid coarsening in the NGG specimen is responsible for the poor creep properties similar to the creep properties of single phase, cast NiAl (curve 1 in the figure). On the other hand, the considerable increase in grain size combined with fine dispersoid size in the SRx specimens is responsible for the improved creep resistance. Partially SRxed specimens (SRx+NGG), which were occasionally produced during the

thermomechanical treatments, show large creep strains and a high creep rate due to the poor creep properties of the NGG areas in the specimen.

The shapes of crept specimens, which were tested at 850°C and 110 MPa for 20 hours, are presented in Fig. 6. As can be seen, there is very little shape change in the SRx specimen, whereas the NGG specimen shows barreling and a significant decrease in length and increase in surface area. The partially recrystallized specimen (SRx+NGG) shows NGG material in the center area, extruded from the sample.

SRx specimens for compression typically consist of less than 5 grains with each grain running the full length of the specimen.

3.2. Creep Mechanisms in SRxed MA NiAl

The steady state creep rate ($\dot{\varepsilon}_s$) and the total creep strain for SRxed specimens are shown in Table 2.

Table 2. Steady State Creep Rates (sec^{-1}) for SRxed MA NiAl

	40 MPa	110 Mpa	180 Mpa
800°C		1.6×10^{-8} (0.55%)*	
850°C		6.6×10^{-8} (0.88%)* 4.0×10^{-8} (0.90%)	
900°C	6.59×10^{-9} (0.9%)	8.6×10^{-8} (1.43%)* 7.2×10^{-8} (1.70%)	4.57×10^{-7} (31%)

Note: * denotes 2nd set of SRx specimens, the numbers in parenthesis indicate the total creep strain in 20 hrs.

The total creep strains are less than 2% over the whole temperature range at 40 and 110MPa, and 31 % at 180 MPa and 900°C.

In order to characterize the creep mechanisms, the activation energy and the creep exponent were calculated based on the creep data. The apparent activation energy for creep (Q_{app}) was obtained from an Arrhenius plot of $\ln \dot{\varepsilon}_s$ versus 1/T at constant stress, Fig. 7;

$$Q_{app} = -R(\frac{\partial \ln \dot{\varepsilon}_s}{\partial (1/T)})_{110MPa} = 177 kJ/mole$$

The stress exponent (n) was also estimated from the plot of $\ln \dot{\varepsilon}_s$ versus $\ln \sigma$ at constant temperature, Fig. 8;

$$n = \left(\frac{\partial \ln \dot{\varepsilon}_s}{\partial \ln \sigma}\right)_{900°C} = 3.05$$

The apparent activation energy for creep in SRx MA NiAl is almost the same as the activation energy (175kJ/mole) in the as-extruded condition [12], but the apparent stress exponent for the SRx condition is higher than that (n=2) for as-extruded condition. The activation energy obtained in this study is in the range of the activation energy for the self diffusion of Ni (150 kJ/mole~250 kJ/mole) in NiAl [13,14], indicating that the creep process is controlled by diffusion regardless of the dominant creep mechanisms [15, 2].

The creep behavior in SRxed MA NiAl is considered to be controlled by dislocation creep mechanism, since the stress exponent (n=3.05) is consistent with this mechanism [16,17,18]. No apparent grain size effect is expected in dislocation creep [11], however, minimum creep rates are in SRx MA NiAl significantly lower than in its as-extruded counterpart [12]. The creep rates decrease between one and two orders of magnitude in the SRxed condition. This suggests that the grain boundary sliding mechanism [19], which is believed to be accommodated by dislocation creep in the as-extruded condition, is suppressed by a reduction in the numbers of grain boundaries and results in lower creep rates. Obviously enough, in addition to the grain size effect, the inherently fine dispersoid size in the SRxed condition is believed to play an important role during creep; dispersoid coarsening leads to increased creep rates in the NGG condition.

Creep of conventional dispersion strengthened materials is characterized by i) high values of apparent activation energy for creep, ii) abnormally high values of stress exponent (n~40), and iii) the existence of a threshold stress (σ_{th}) below which no measurable creep rate can be detected [20, 21, 2]. Lund and Nix suggested that the abnormally high values of Q_{app} were attributable to the temperature dependence of the elastic modulus and the abnormally high values of n in DS materials [20]. The abnormally high n value in DS alloys arises from the presence of a threshold stress which is believed to originate from the resistance to dislocation motion by particles [2,3,22]. In a clear contrast to conventional DS counterparts, SRxed MA NiAl does not exhibit an abnormally high apparent activation energy for creep or apparent stress exponent. This is in part due to the relatively insensitive temperature dependence of the elastic modulus in NiAl [23, 24], and the low threshold stress value observed in as-consolidated MA NiAl [12].

In order to rationalize the elastic modulus effect on Q_{app}, the true activation energy (Q_C) for creep was estimated using the elastic modulus compensated creep equation proposed by Shelby [25]. The equation is given by;

$$\dot{\varepsilon}_s = A' \left(\frac{\sigma}{E(T)}\right)^{n'} \exp\left(-\frac{Q_c}{RT}\right)$$

Since the creep rate of many ODS alloys is determined by an effective stress (σ-σ_{th}) [21, 2], the normalized creep equation with respect to the effective stress is generally expressed by;

$$\dot{\varepsilon}_s = A_0 \left(\frac{\sigma - \sigma_{th}}{E(T)} \right)^{n_0} \exp\left(-\frac{Q_c}{RT} \right)$$

where A_0 is a structural dependence constant and n_0 is the true stress exponent, Q_C is true activation energy and other parameters have their usual meaning. The true stress exponent, n_0, can be normalized with respect to the apparent n;

$$n_0 = n \frac{\sigma - \sigma_{th}}{\sigma} = n \left[1 - \left(\frac{\sigma_{th}}{\sigma} \right) \right]$$

As can be seen, the apparent n value will increase for any finite value of σ_{th}, and the larger the σ_{th} the larger the n value for a given σ. From the equations, Q_C can be derived by;

$$Q_c = -R \left[\frac{\partial \ln \dot{\varepsilon}_s}{\partial (1/T)} \right]_\sigma - nR \frac{d \ln E(T)}{d \ln(1/T)} = Q_{app} + nR \frac{T^2}{E} \frac{\partial E}{\partial T}$$

Assuming no significant differences in elastic modulus between SRx and as-extruded condition, an elastic modulus equation which was experimentally determined for <110> oriented single crystal NiAl [26] was applied in this calculation;

$$E(T) = 195.055 - 0.0349T (GPa)$$

where T is in K. Based on this equation, the E(900°C) and $\partial E/\partial T$ (900°C) were found to be 154.1 GPa, -0.0349 GPa/K, respectively. Using n=3.05 and Q_{app}=177kJ/mole, the true activation energy was estimated to be 169.1 kJ/mole. Thus the Q_{app} measured in SRxed MA NiAl is very similar to the true value because of the relatively insensitive temperature dependence of the elastic modulus. A similar result was shown in a previous creep study for as-extruded MA NiAl in which Q_{app} and Q_C were found to be equal to 175 and 174.2 kJ/mole, respectively [12].

3.3. Threshold Stress Behavior

Since the stress exponent in SRxed condition is in the normal range for dislocation creep mechanism, the threshold stress is expected to be small. However, it is necessary to examine the threshold stress behavior in this material since the creep rate of many ODS alloys is determined by an effective stress ($\sigma - \sigma_{th}$) [27, 21, 2]. The threshold stress can be measured by either a load reduction test at constant temperature[28] or a graphical method [29, 3], and the estimated threshold stress by the graphical method shows good correlation with measured threshold stress in the as extruded MA NiAl [12]. In this study, an estimation of the threshold stress for SRxed MA NiAl was made using the graphical method.

From the normalized creep equation, the threshold stress can be estimated by extrapolating a linear plot of $[\dot{\varepsilon}_s/A_0 \exp(-Q_c/RT)]^{1/n_0}$ versus $\sigma/E(T)$ to the zero values of normalized stress [3]. For the plot, n_0 is generally preset to the normal value of n for dislocation creep (n=4) in the ODS alloys which have abnormally high n value [3], but the n_0 can be set to

3.05 in this case since the apparent stress exponent is in the normal range of dislocation creep. Q_c is set to 169.1 kJ/mole, and A_o is determined from the rearranged creep equation using experimental creep data;

$$\dot{\varepsilon}_1^{\frac{1}{n_o}} - \dot{\varepsilon}_2^{\frac{1}{n_o}} = A_0^{\frac{1}{n_o}} \frac{(\sigma_1 - \sigma_2)}{E(T)} \exp(-\frac{Q_c}{n_o RT})$$

Using the data, a linear plot of $[\dot{\varepsilon}_s/A \exp(-Q/RT)]^{1/n}$ versus $\sigma/E(T)$ was made, Fig. 9. and the zero intercept value was found to be $\sigma_{th}/E_{900°C} = 2.2 \times 10^{-5}$. Hence, putting $E_{900°C} = 154.1$ GPa, the estimated threshold stress for SRx MA NiAl at 900°C is found to be 3.4 MPa. Given experimental errors, this result implies that σ_{th} is negligible in the SRx condition. As a reference, σ_{th} in as-extruded MA NiAl was found to be about 20 MPa [12].

The origin of the threshold stress in as-extruded condition was considered to be the threshold stress for localized dislocation climb under equilibrium conditions over non-attracting particles [12]. This model was proposed by Rösler and Arzt [30], and provides the best estimate of the threshold stress in MA NiAl among the currently available models. The threshold stress proposed by the model is given by:

$$\frac{\tau_{th}}{\tau} = \frac{h}{l}$$

where h is the particle height (~particle radius), l is planar spacing of the particles. The threshold stress can be expected to decrease with particle coarsening assuming no change in volume fraction during the test. Thus the lower value of threshold stress in the SRxed condition can be attributed to dispersoid coarsening during SRx. It has been suggested that threshold stress could depend on grain size through the fluctuation of boundary area when the grain boundary sliding accommodation process was considered [31]. In this model, the threshold stress is considered to be the stress necessary to enable deformation to continue and is estimated to be ~$0.72\gamma/d$, where d is grain size.

Using the estimated threshold stress, the stress exponent, which was initially set to 3.05, can be verified from the diffusion compensated, normalized creep equation in the form of;

$$\frac{\dot{\varepsilon}_s}{D} = A_0 [\frac{(\sigma - \sigma_{th})}{E(T)}]^{n_o}$$

The diffusion compensated, normalized plot is presented in Fig. 10 and n_0 was found to be 3.02 which is almost identical to the apparent stress exponent (n=3.05). This implies that the apparent creep parameters are not very different from the true values due to the low value of threshold stress in SRxed MA NiAl. In the figure, the plot for as-extruded specimens [12] is also presented for comparison. As can be seen, in comparison to the creep of as-extruded condition, the true stress exponent increases from 1.42 to 2.46, and the effective creep rate was decreased one or two orders of magnitude by secondary recrystallization. The increase in true stress exponent implies that the contribution of grain boundary sliding accommodation to the dislocation creep in MA NiAl is greater in the fine grained as-extruded condition because the n_0 in the as extruded

A-8

condition is close to 1 (diffusional creep), but the contribution becomes smaller due to the reduction of grain boundaries in the SRx condition leading to higher values of n_0.

3.4. Effect of macrostructure on creep

Compressive creep properties of SRxed MA NiAl at 900°C are compared with the creep data for the as consolidated MA NiAl tested at 900 °C and published creep data for NiAl tested at 927°C (1200 K), Fig. 11. Creep properties of MA NiAl were shown to be enhanced by mechanical alloying process in comparison with their cast counterpart or other DS NiAl produced by Rapid Solidification Technology. SRx specimens having a coarse grain structure with fine dispersoid were shown to exhibit significantly improved creep properties. The grain aspect ratio in the SRxed specimens was about 4 with full grain length parallel to the stress axis, whereas all of the other materials were equiaxed. It has been shown that the high temperature strength and the threshold stress generally increase with increasing grain aspect ratio in DS materials [1] due to the minimization of grain boundary sliding by reduction of the number of grain boundaries with an imposed shear stress. In addition, high grain aspect ratio morphology can reduce cavity formation and growth as proposed by Arzt and Singer, leading to reduction in creep rates [32]. Arzt and Singer suggested that cavity growth on transverse boundaries (in tension) produces incompatibilities between neighboring grains but it can be eliminated by local grain boundary sliding in the longitudinal direction [32]. However, such an improvement in creep properties by minimizing cavitation in high grain aspect ratio is not expected in compression mode [33, 34].

It is also reported that the creep rates will be significantly different depending on testing modes especially in small sized and equiaxed specimens [33]. Timmins and Arzt have shown that creep parallel to the longitudinal grain direction of MA6000 (high grain aspect ratio structure) in tension is similar to that in compression whereas transverse creep in tension is considerably worse in comparison to compression mode in which cavitation is almost completely suppressed [33]. In other words, an increase in the number of transverse grain boundaries (as in small grain size) resulted in considerable creep rate enhancement in tension, while such a change was not observed in compression. Although the cavitation mechanism is not expected in compression creep mode, the minimization of grain boundary sliding by reduction of grain boundaries under the shear stress can still be of significance in compression creep [33].

NiAl can give a reduction in weight by as much as 40% with consequent reduction in centrifugal stress in comparison to current superalloys for gas turbine engine applications. For this reason, comparison of mechanical properties by density compensation was madd. The density compensated creep rate of SRxed MA NiAl at 900°C is comparable to some superalloys, Fig. 12.

3.5. Summary

The results of the reported studies are summarized below.

1.   Microhardness of MA NiAl as a function of grain size and dispersoid spacing obey Hall-Petch type relations, with stronger correlation with dispersoid spacing than with grain size. Microhardness and hot compression results show that SRx materials are superior to the material grain coarsened by normal grain growth. Although the assessment of ductility is

only qualitative the results from this work suggest that fine dispersoid might be used for ductility enhancement in MA NiAl without the necessity of a fine grain size.

2. Enhanced dispersoid coarsening during normal grain growth led to poor creep properties similar to single phase NiAl, despite an increase in grain size. On the other hand, pronounced grain coarsening and high grain aspect ratio combined with fine dispersoid size produced by SRx result in improved creep resistance in comparison to creep in both the as-extruded condition and the normal grain growth condition.

3. The apparent activation energy and stress exponent for creep in SRx MA NiAl were found to be 177 kJ/mole and 3.05, respectively. The Q_{app} appears to be in the range of the activation energy for self diffusion and the values of the stress exponent and Q_{app} point to dislocation creep controlled by climb, as prevailing creep mechanism. The minimum creep rate in SRx material was decreased one or two orders of magnitude in comparison to creep in the as-extruded condition. This indicates a contribution from grain boundary sliding to the creep rate of these materials.

4. The threshold stress is negligible in SRx MA NiAl. This is attributed to larger dispersoids compared to the extruded materials and a decrease in grain boundary area.

5. Secondary recrystallization of dispersion strengthened intermetallics offers a potential processing route for optimization of the high temperature mechanical properties.

4. REFERENCES

[1] B. A. Wilcox and A. H. Clauer, "The Role of Grain Size and Shape in Strengthening of Dispersion Hardened Nickel Alloys", Acta Metall., 20, pp. 743-757, (1972).

[2] C. M. Sellars and R. A. Petkovic-Luton, "Creep of Dispersion Strengthened Alloys", Mater. Sci. and Eng., 46, pp. 75-87, (1980).

[3] T. E. Howson, J. E. Stulgar and J. K. Tien, "Creep and Stress Rupture of Oxide Dispersion Strengthened Mechanically Alloyed Inconel Alloy MA 754", Metall. Trans., 11A, pp. 1599-1607, (1979).

[4] S.C. Ur, "A Study of Normal Grain Growth, Secondary Recrystallization, and High Temperature Properties in Mechanically Alloyed NiAl", Ph. D. Thesis, IIT, Chicago, Il., (1994).

[5] M. Dollar, S,. Dymek, S. J. Hwang and P. Nash, "The Occurrence of <110> Slip in NiAl", Scripta Metall., 26, pp. 29-34, (1992).

[6] J. D. Whittenberger, R. K. Viswanadham, S. K. Mannanand K. S. Kumar, "1200 to 1400 K Slow Strain Rate Compressive Behavior of Small Grain Size $NiAl/Ni_2AlTi$ alloys and $NiAl/Ni_2AlTi-TiB_2$ Composites", J. of Mater. Res., 4, 5, pp. 1164-1171, (1989).

[7]   H. Mecking and G. Gottstein, "Recovery and Recrystallization during Deformation", Recrystallization of Metallic Materials, F. Haessner, ed., Dr. Riederer Verlag GmbH, Stuttgart, Germany, pp. 195-222, (1978).

[8]   M. Dollar, S. Dymek, S. J. Hwang and P.Nash, "The Role of Microstructure on Strength and Ductility of Hot Extruded MA NiAl", Metall. Trans., 24A, pp. 1993-2000, (1993).

[9]   J. B. Breedis, B. A. Koss, J. Poole and I. Locci, "NiAl-Fe+Y_2O_3 Alloys Processed by Mechanical Alloying", Proc. of 2nd Int. Conf. on Structural Application of MA, F. H. Froes, J. J. deBarbadillo and J. D. Whittenberger, eds., ASM International, pp. 275-281, (1993).

[10]   G. E. Dieter, "Mechanical Metallurgy", 2nd ed., McGraw -Hill, (1976).

[11]   R. W. Hertzberg, "Deformation and Fracture Mechanism of Engineering Materials", 3rd ed., John-Wiley and Sons, (1989).

[12]   S. Suh, "Creep in Mechanically Alloyed NiAl Based Materials", Ph.D Thesis, IIT, Chicago, IL, (1994).

[13]   A. Lutze-Birk and H. Jacobi, "Diffusion of ^{114m}In in NiAl", Scripta Metall., 9, pp. 761-765, (1975).

[14]   S. Shankar and L. L. Seigle, "Interdiffusion and Intrinsic Diffusion in the NiAl (δ) Phase of the Al-Ni System", Metall. Trans, 9A, pp. 1467-1476, (1978).

[15]   J. Weertman, "Theory of Steady State Creep Based on Dislocation Climb", J. Appl. Phys. 26, pp. 1213-1217, (1955).

[16]   O. D. Sherby and P. M. Berke, "Mechanical Behavior of Crystalline Solids at Elevated Temperature", Proc. Mater. Sci., 13, pp. 325-390, (1968).

[17]   J. Weertman, "Dislocation Climb Theory of Steady State Creep", Trans. ASM, 61, pp. 681-693, (1968).

[18]   M. V. Nathal, "Creep Deformation of B_2 Aluminides", Ordered Intermetallics, C. T. Liu, ed. Kluwer Academic Publishers, pp. 541-563, (1992).

[19]   R. Raj and M. F. Ashby, "On Grain Boundary Sliding and Diffusional Creep", Metall. Trans., 2, pp. 1113-1127, (1971).

[20]   R. W. Lund and W. D. Nix, "On High Creep Activation Energies for Dispersion Strengthened Metals", Metall. Trans., 6A, pp. 1329-1333, (1975).

[21]   J. D. Whittenberger, "Creep of Tensile Properties of Several Oxide Dispersion Strengthened Nickel Base Alloys", Metall. Trans., 8A, pp. 1155-1163, (1977).

[22]   V. C. Nardone, D. E. Matejczyk and J. K. Tien, "Creep of Oxide Dispersion Strengthened Materials", Acta Metall., 32, 9, pp. 1509-1517, (1984).

[23]   D. B. Miracle, "The Physical and Mechanical Properties of NiAl", Acta Metall., 41, 3, pp. 649-684, (1993).

[24]   R. D. Noebe, R. R. Bowman and M. V. Nathal, "Review of the Physical and Mechanical Properties and Potential Applications of the B_2 NiAl", Int. Mater. Rev., 38, pp. 193-232, (1993).

[25]   O. D. Sherby, "Factors Affecting the High Temperature Strength of Polycrystalline Solids", Acta Metall., 10, pp. 135-147, (1962).

[26]   R. J. Wasilewski, "Elastic Constants and Young's Modulus of NiAl", Metall. Trans., 236, pp. 455-457, (1966).

[27]   B. Burton, "Vacancy Flow as a Deformation Mechanism in Polycrystals", Vacancies '76, R. E. Smallman and J. E. Harris, Metal Society, London, England, pp. 156-169, (1976).

[28]   J. D. Parker and B. Wilshire, "The effect of a Dispersion of Cobalt Particles on High Temperature Creep of Copper", Metall. Sci. J., 9, pp. 248-252, (1975).

[29]   S. Purushothaman and J. K. Tien, "Role of Back Stress in the Creep Behavior of Particle Strengthened Alloys", Acta Metall., 26, pp. 519-528, (1978).

[30]   J. Rösler and E. Arzt, "The kinetics of Dislocation Climb over Hard Particles": part I "Climb without Attractive Particle-Dislocation Interaction", Acta Metall., 36, 4, pp. 1043-1051, (1988).

[31]   M. F. Ashby and R. A. Verrall, "Diffusion Accommodated Flow and Superplasticity", Acta Metall., 21, pp. 149-163, (1973).

[32]   E. Arzt and R. F. Singer, "The Effect of Grain Shape on Stress Rupture of the Oxide Dispersion Strengthened Superalloys Inconel MA6000", Proc. of 5th Int. Symp. on Superalloys, TMS of AIME, pp. 367-376, (1984).

[33]   R. Timmins and E. Arzt, "The Transverse Creep Behavior of MA6000 in Tension and Compression, Structural Application of Mechanical Alloying", F. Froes and J. J. deBarbadillo, eds., ASM International, pp. 67-77, (1991).

[34]   J. D. Whittenberger, R. Ray and S. C. Jha, "Influence of Grain Size on the Creep Behavior of HfC-Dispersed NiAl", Mater. Sci. and Eng., A151, pp. 137-146, (1992).
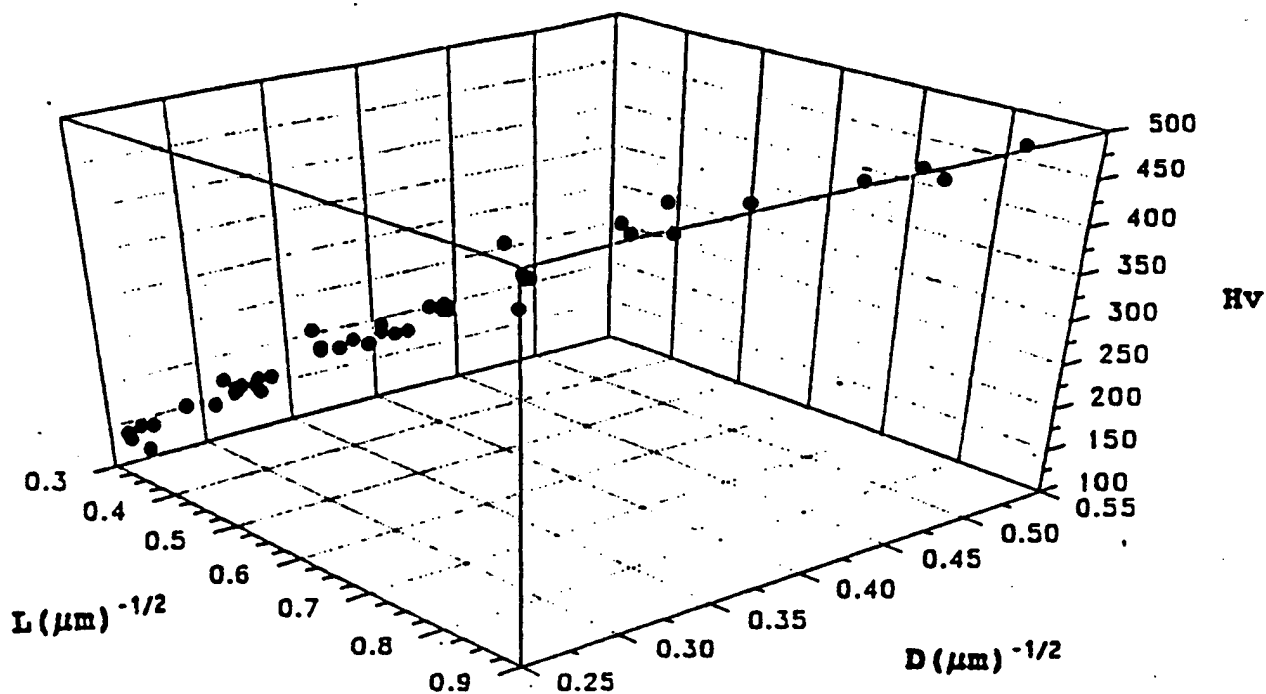
Fig. 1.   Microhardness as a function of grain size (D) and dispersoid spacing (L).
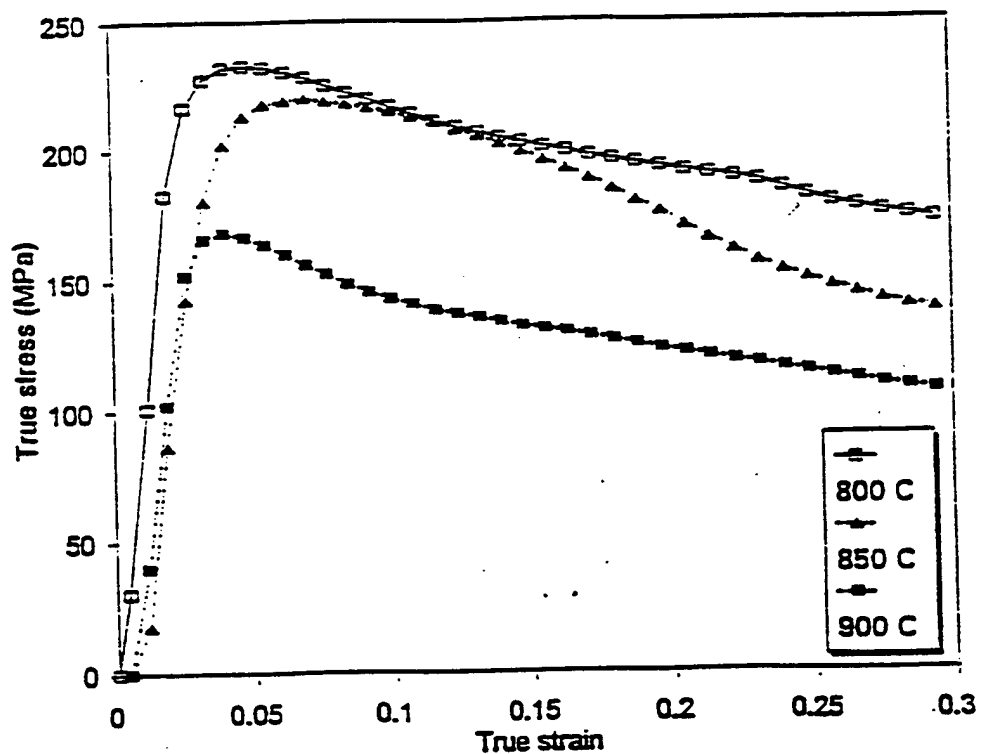
Fig. 2.   High temperature compressive flow curves of SRxed MA NiAl.
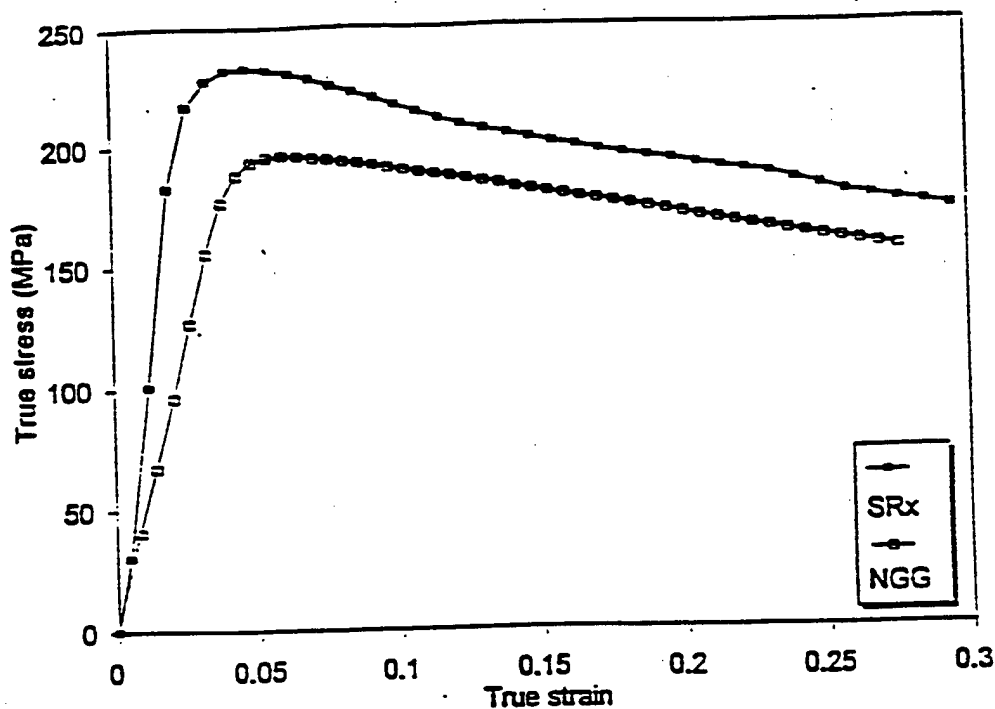
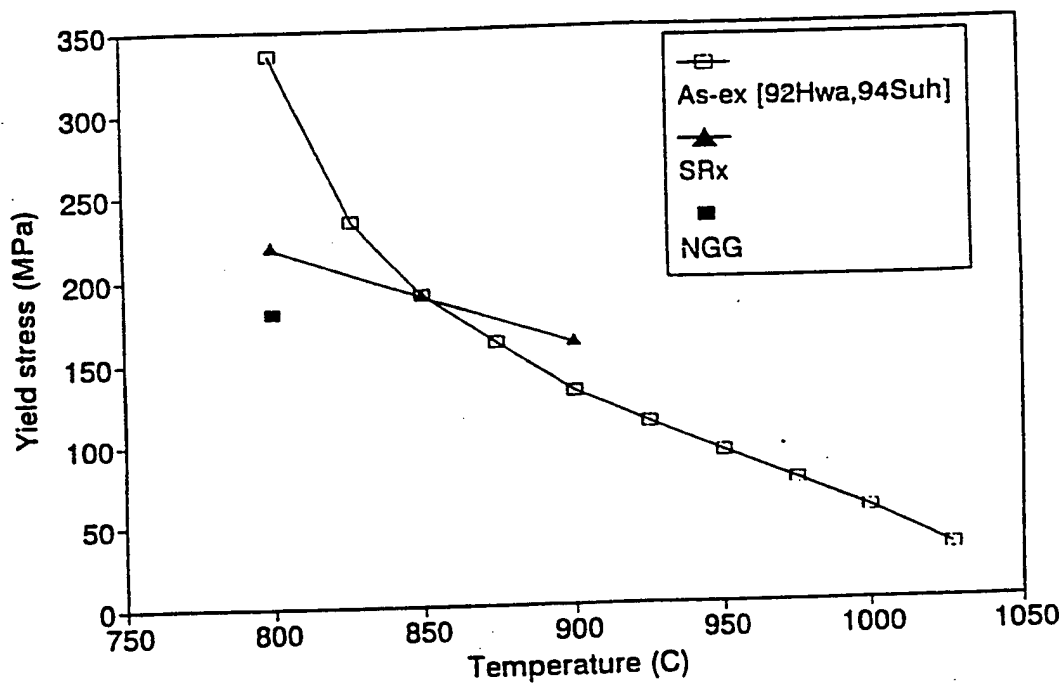Fig. 3.   Compressive flow curves for NGG and SRx MA NiAl tested at 800°C

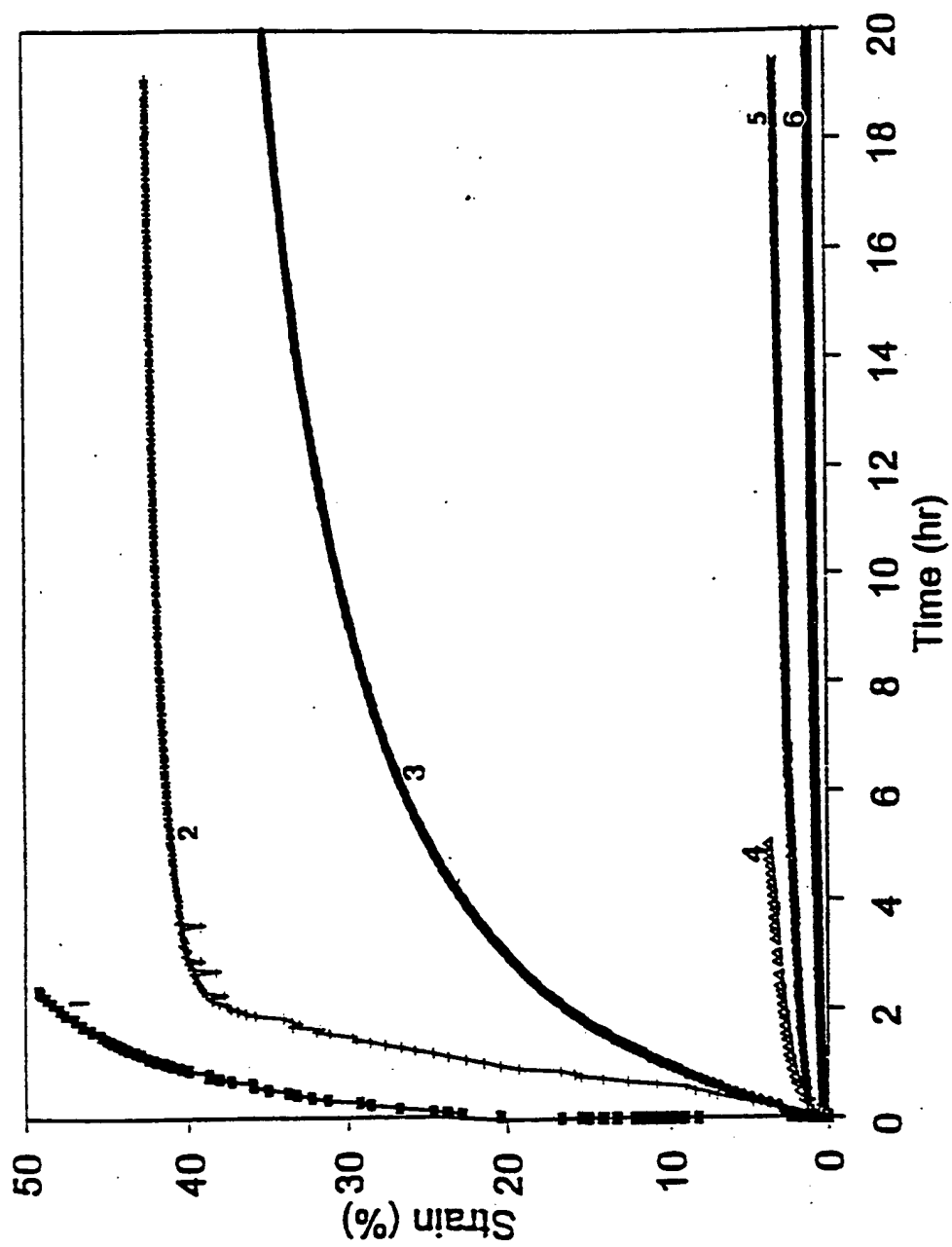Fig. 4.   Grain coarsening effect on 0.2% offset yield stress as a function of temperature.
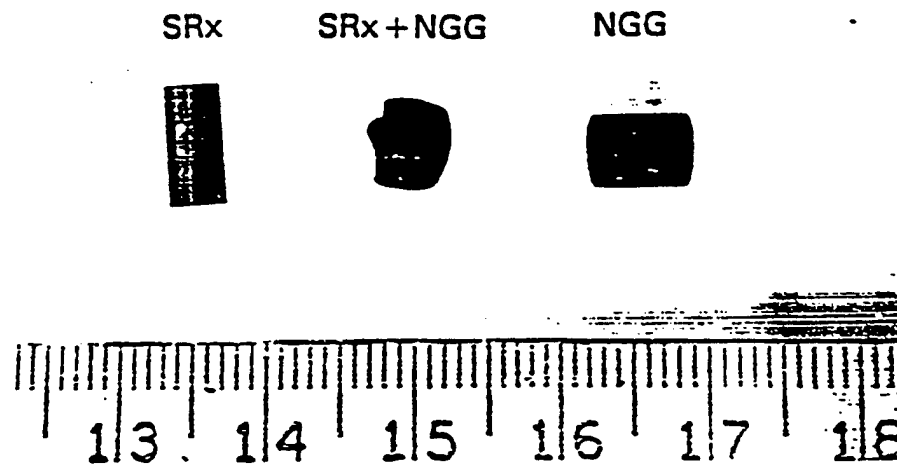
Fig. 5.Creep curves in MA NiAl at 110 MPa and 850°C.

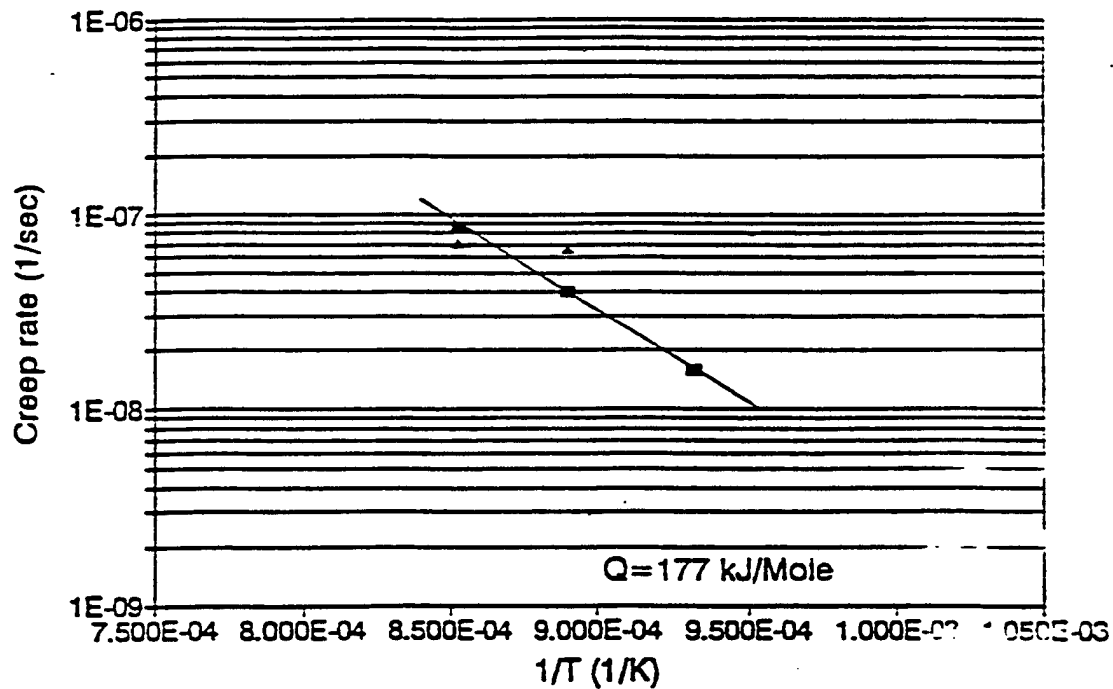Fig. 6.   Shapes of the crept specimens of MA NiAl, tested at 110 MPa and 850°C for
           20 hours (compression axis is vertical).

Fig. 7.   Arrhenius representation of the temperature dependence of mi.....num creep rate
           at 110MPa in SRxed MA NiAl.
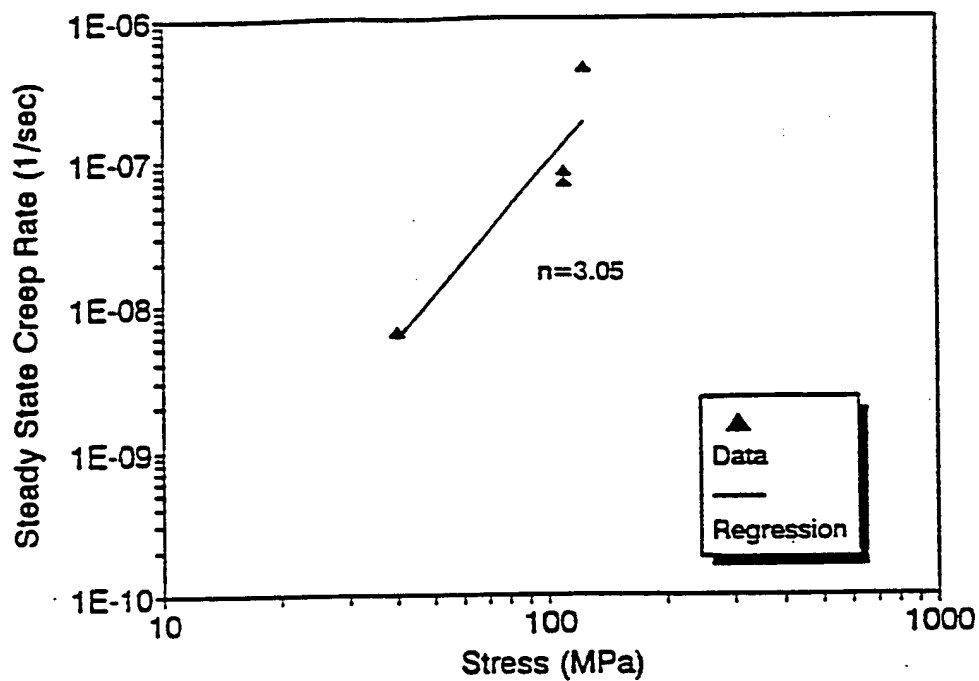
Fig. 8.   Stress dependence of minimum creep rate of SRxed MA NiAl at 900°C.
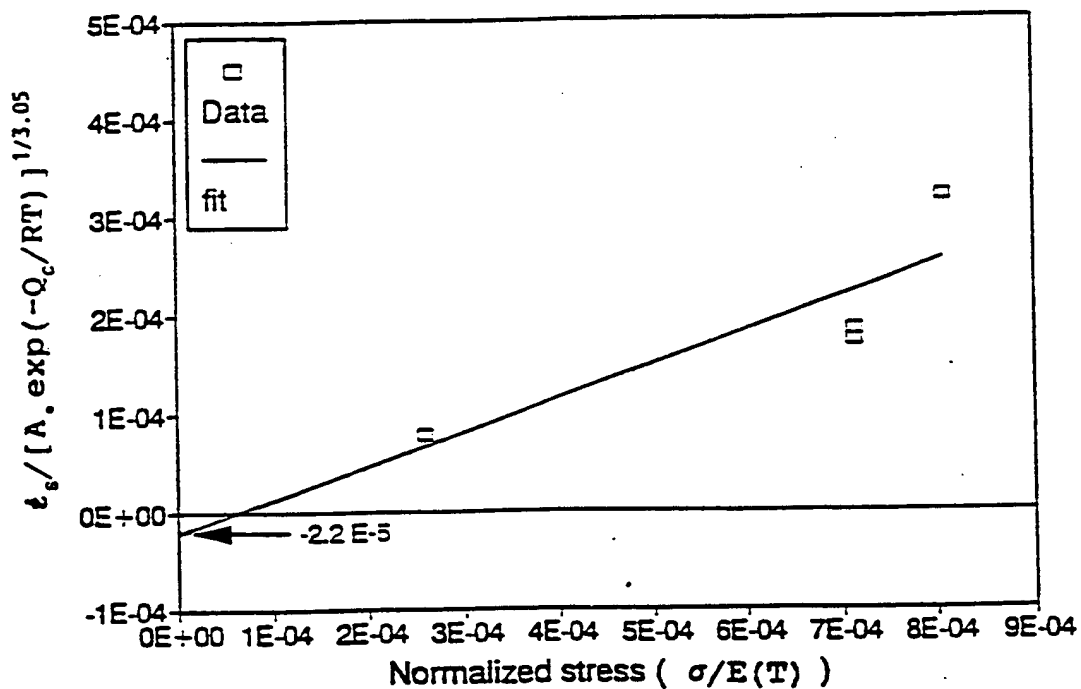
Fig. 9.   A linear plot of $[\dot{\varepsilon}_s/A_o \exp(-Q_c/RT)]^{1/n}$ versus $\sigma/E(T)$ for the threshold stress calculation.
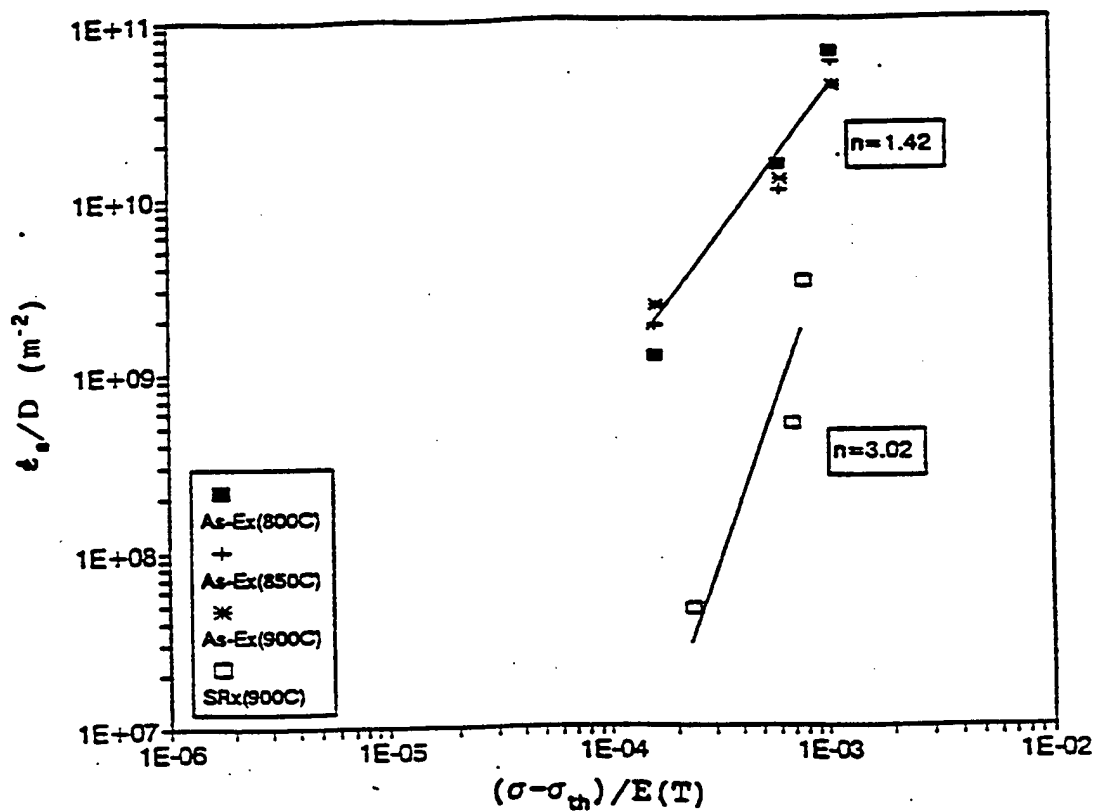
Fig. 10.   Diffusion compensated creep rate as a function of modulus compensated effective stress for MA NiAl.
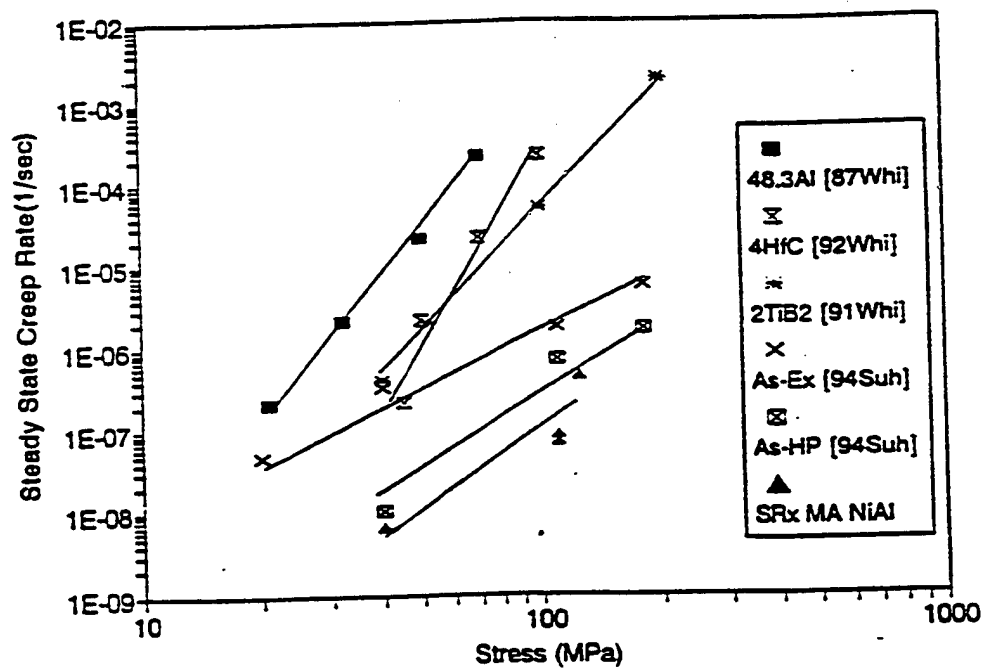

Fig. 11.   Comparison of creep properties of SRxed MA NiAl with other dispersion strengthened NiAl: as-Ex, as-HP and SRx MA NiAl were tested at 900°C, and others were at 927°C.
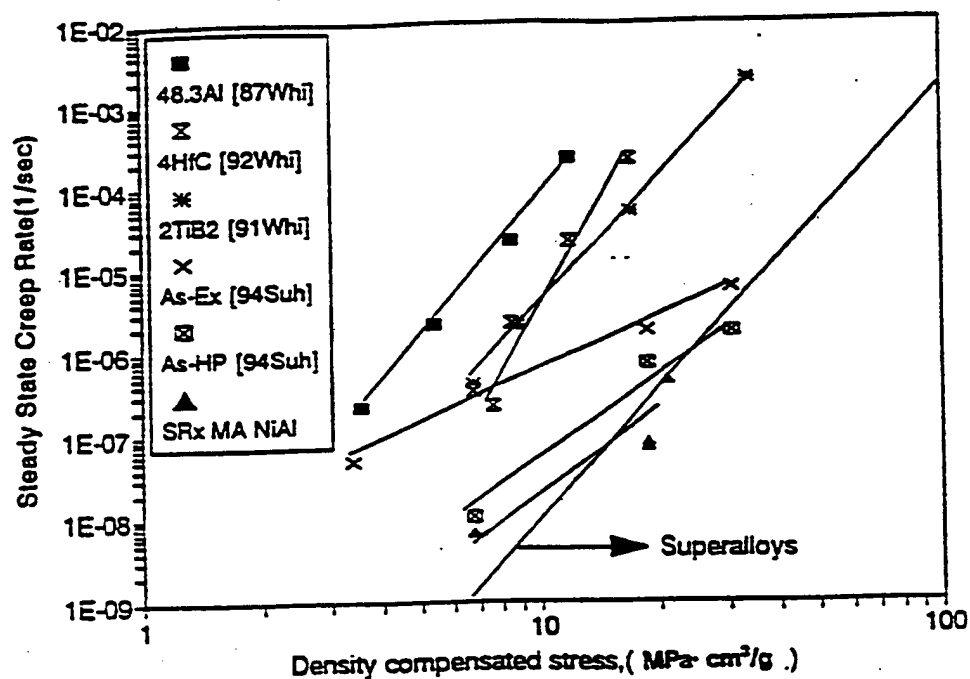
Fig. 12.   Comparison of density-compensated creep properties at 1200 K: as-Ex, as-HP and SRx MA NiAl were tested at 900°C and others were tested at 927°C (1200 K).
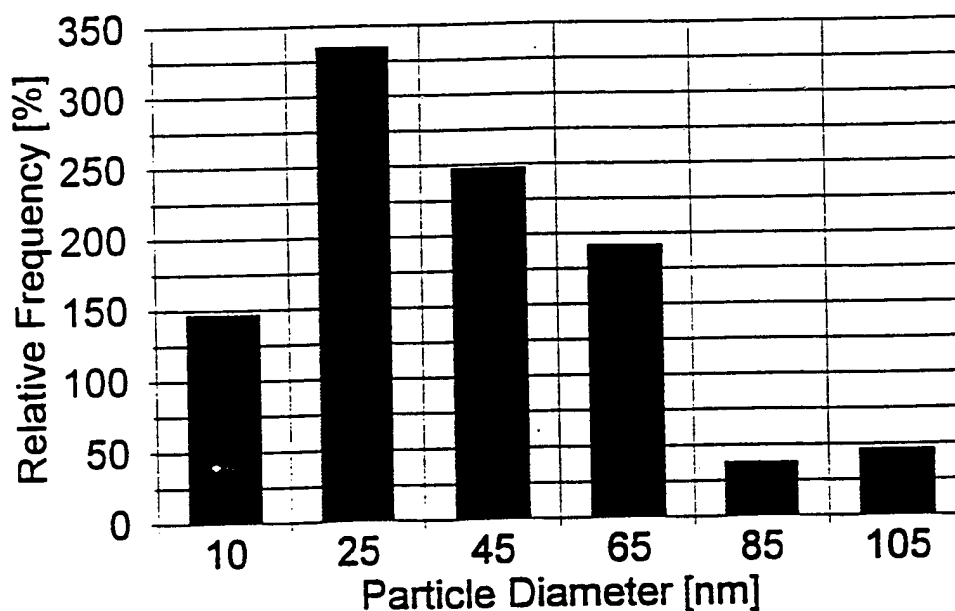
Particle Size Distribution

Fig. 13.   Particle size distribution in the SRx specimen.

PART B : NiAl-BASED FIBER-REINFORCED COMPOSITES

1300K COMPRESSIVE BEHAVIOR OF NiAl-AlN-Al₂O₃ COMPOSITES

1. INTRODUCTION

NiAl and NiAl-based alloys have been recognized as potential high temperature structural materials because of their attractive properties such as low density, high melting temperature, high thermal conductivity and excellent oxidation resistance [1,2]. However, the structural application of NiAl and its alloys is not possible at this time primarily due to their inherent brittleness and lack of fracture toughness at ambient temperature and poor creep resistance. A great deal of research has been focused on addressing these problems but an adequate balance of ambient temperature fracture toughness and high temperature strength have not yet been achieved.

Currently developed AlN dispersion strengthened NiAl materials processed by cryomilling [3-5] or mechanical alloying (MA) [6-7] show excellent high temperature strength and are a potential replacement for current high temperature structural materials such as superalloys. Recently fiber-reinforced NiAl-based composites have been recognized as a viable route for improving both high temperature properties and room temperature toughness [8-12]. In order to achieve an adequate balance of room temperature fracture toughness and high temperature strength, a hybrid NiAl composite containing both AlN dispersion particles and Al₂O₃ fibers has been developed [7]. AlN dispersoid particles not only improve the high temperature strength and oxidation resistance of NiAl but also may affect the bonding characteristics at the fiber/matrix interface. The presence of the dispersoid particles in the matrix may reduce the coefficient of thermal expansion (CTE) mismatch at the interface [6]. The key factors in the selection of a suitable fiber-reinforcement material are : (1)the chemical compatibility of the fiber with the matrix [13] and (2)close match in CTE between the fiber and the matrix. Although there are several reinforcement materials which are chemically compatible with NiAl alloys, there are only a few among these which have a CTE matched closely to that of NiAl alloys. The thermal expansion coefficients for many of the compatible reinforcement materials are much lower than that of NiAl alloys. Furthermore, relatively few types of fibers are commercially available. This severely restricts the choice of potential reinforcement materials. Considering these parameters, Al₂O₃ fiber has been selected as the reinforcement material.

In this paper the 1300K compressive strengths of NiAl-based composites containing both 5 vol. % AlN and various vol. % of Al₂O₃ fibers are presented.

2. EXPERIMENTAL PROCEDURES

NiAl powder containing 5.6 vol. % AlN dispersion was synthesized by mechanical alloying (MA) of elemental nickel and aluminum powder under nitrogen atmosphere [6,7]. Nextel 610 fiber (Al₂O₃ , >99 wt.% ; density = 3.88 g/cm³) manufactured by 3M [14] was obtained in the form of short fibers with an average diameter of 12 μm and length of 3.2 mm (aspect ratio 1:267). Composites were fabricated by hot pressing a dry blend of the as-milled NiAl powder containing

5 vol. % AlN dispersion and 0, 5,15 or 30 vol. % of Al_2O_3 fibers. The hot pressing of the composites was performed at 1473K and 120MPa for 3 hours in an argon atmosphere [15]. Once hot pressing was finished the sample was unloaded and furnace cooled to room temperature. Fig. 1 illustrates the composite processing route. It should be noted that the ratio of NiAl to AlN was constant at 95:5 while the Al_2O_3 volume percentage changes from 0, 5,15 to 30%.

The microstructure of the as hot pressed composites as well as their monolithic counterpart were examined using optical microscopy and transmission electron microscopy (TEM). TEM samples were prepared from discs sectioned perpendicular to the hot pressing axis. The thin foils were prepared by grinding, polishing and dimpling followed by ion milling under a typical condition of 5kV gun voltage, 3mA gun current and 12° specimen tilt angle. TEM investigation was carried out using a Philips CM 200 operating at 200kV.

Rectangular cross-sectioned compression test specimens ($3x3x6 mm^3$) were machined from hot pressed composites by wire-EDM from the monolithic material and by diamond grinding from the composites, with the length parallel to the hot pressing direction. The constant velocity compression tests were carried out in air at 1300K at nominal strain rates of $8.5x10^{-4}$, $1x10^{-4}$, $1x10^{-5}$ and $2.8x10^{-6}$ sec^{-1} using a modified Instron universal testing machine [16]. The load-displacement data were converted to true compressive stress-strain assuming conservation of sample volume [17]. Constant load compressive creep tests were also performed on the 0% and 30% composites at 1300K and 110 MPa in air using a modified SATEC M-3 creep system equipped with SiC push rods. The time-displacement data were translated into creep curves following methods described elsewhere [18].

3. RESULTS AND DISCUSSION

3.1. Microstructure

Optical micrographs of the as-hot pressed materials, Fig.2, showed that all materials are fully dense and free from cracks. Typical microstructure of NiAl matrix, Fig.2(a), shows a relatively homogeneous distribution of second phase particles (darker regions) in the NiAl matrix. However, dispersion scarce regions (marked arrow) are also observed in the matrix and the typical volume percentage of this feature is determined as less than 1 % by point counting method. These regions are likely associated with partially processed MA powders [19]. The second phase particles were identified as AlN (and also small amount of Al_2O_3) by using X-ray and electron diffraction and energy dispersive spectrometry [7]. The microstructure of the 30% composite, Fig.2(b), shows a homogeneous distribution of randomly oriented fibers in the matrix. Few pores were visible in the matrix and at the fiber/matrix interface (typically less than 2 volume percent in the 30% composite), and the fiber bonded well with the matrix without any cracks being observed, Fig.2(c).

TEM images of the matrix, Fig.3(a), confirmed that the dispersoid particles (marked arrow) are distributed quite homogeneously throughout the NiAl matrix (marked A). The NiAl grains and second phase particles have quite a broad range of sizes. Most of the NiAl grains are within the size range of 0.1 to 0.7 μm, but a few large grains (1~3 μm) were also observed.

B-2

While many of the small NiAl grains are particle-free, larger grains contain dispersoid particles within the grains. The dispersoid particle size is bimodal and small particles range from 10 to 150nm dispersed throughout the matrix and larger ones range from 0.1 to 0.7μm preferentially distributed at the grain boundaries. Fig.3(b) shows that while the AlN particles (marked B) are distributed both within the NiAl grains and at the grain boundaries, the Al_2O_3 particles (marked C) tend to reside along the grain boundaries. TEM studies of the as-hot pressed composites revealed that the fiber bonded very well with both the NiAl grains, Fig.4(a), and dispersoid particles, Fig.4(b), i.e. no cracks or voids were detected. Chemical reaction between fiber and matrix is not evident. While NiAl grain and the fiber always formed quite discrete interfaces, the interface between dispersoid particles and the fiber was occasionally diffuse and obscure. The similarity of the chemical composition between the fiber and the oxide particles may have caused the continuity at the interface. Few dislocations were observed in the small NiAl and Al_2O_3 fibers in as-fabricated composites and only a few very large NiAl grains near fibers, Fig.4(a), showed some dislocations. The energy dispersive analysis in the TEM shows that the NiAl grains in both NiAl-AlN and NiAl-AlN-Al_2O_3 composites have a composition close to stoichiometry (50/50) but nickel rich grains were also frequently observed throughout the specimen. The statistical analysis of NiAl composition and grain size variation as a function of Al_2O_3 fiber vol. % is currently under investigation and will be reported elsewhere.

3.2. Mechanical properties

3.2.1. Compressive stress-strain behavior

The constant velocity compression tests were carried out for NiAl-AlN, NiAl-AlN-5%Al_2O_3 15% and 30% composites in air at 1300K at nominal strain rates of 8.5×10^{-4}, 1×10^{-4}, 1×10^{-5} and 2.8×10^{-6} sec^{-1}. True compressive stress-strain curves of NiAl-AlN-Al_2O_3 composites at 1300K as a function of strain rate and Al_2O_3 fiber vol. % are shown in Fig.5. In all cases, the flow stress increased with increasing strain rate. For the 0, 5, 15% composites yielding was followed by work hardening. Once the stress reaches the maximum value, either strain softening (strain rate $\geq 1 \times 10^{-5}$) or constant stress flow ($\leq 1 \times 10^{-5}$) took place at around 2% strain. However, the 30% composite showed strain softening as it reaches its 0.2% offset yield stress at all strain rates.

At the strain rate of 1×10^{-4}, the yield stress of the monolithic NiAl and the 30% composite is measured as 205 and 330 MPa, respectively. The yield strength of the 30% composite is more than 60% greater than its monolithic counterpart and is similar to the yield strength of cryomilled NiAl-30%AlN composite developed by Hebsur et al.[5]. Fig.6 shows the 0.2% compressive yield stress of the composites as well as the matrix at 1300K as a function of the fiber vol. % at various strain rates. It clearly demonstrates that the composite strength increases as the fiber vol. % increases at all strain rates. The data points at each strain rate are fitted to the linear equation

$$\sigma_{cy} = \sigma_{my} + C \, V_f \qquad (1)$$

where σ_{cy} is composite yield stress, σ_{my} is matrix yield stress, V_f is fiber volume fraction and C is the slope of the curve. The regression results, along with the coefficient of determination R_d^2, are shown in Table 1. The results indicate that the yield strength of the composites increases linearly as the fiber vol. % increases. However the effect of the fiber volume fraction on the composite yield strength, i.e. C, is much greater at faster strain rates ($\geq 1 \times 10^{-4}$) than at slower strain rates ($\leq 1 \times 10^{-5}$) where thermally activated processes can play a dominant role. This suggests that the composites are more sensitive to the strain rate than the monolithic material and this behavior can be better explained by analyzing flow stress-strain rate behavior.

Table 1. The linear regression fits of the 0.2% yield stress - Al_2O_3 fiber vol. % relationship for NiAl composites at 1300K and various strain rates

Strain rate (sec^{-1})	σ_{my} (MPa)	C (MPa)	R_d^2
8.5×10^{-4}	255 ± 3	457 ± 22	0.995
1×10^{-4}	196 ± 9	421 ± 57	0.964
1×10^{-5}	149 ± 8	266 ± 52	0.928
2.8×10^{-6}	113 ± 5	264 ± 31	0.973

3.2.2. Constant load creep behavior

Constant load compressive creep tests were also performed on the 0% and 30% composites at 1300K and 110MPa in air. The creep curves showing the true compressive strain-time relation is shown in Fig.7. Primary creep is followed by steady state creep, which begins after about 5 hours. The results show that the steady state creep rate of the 30% composite (2.3×10^{-8} sec^{-1}) is more than one order of magnitude slower than that of the monolithic counterpart (3.1×10^{-7} sec^{-1}).

3.2.3. Strain rate-flow stress behavior

The strain rate-true compressive stress behavior of the composites as well as the matrix was studied by using the data collected from constant velocity compression tests. The 3% flow stress was used when the stress-strain behavior showed constant flow and 0.2% yield stress was used as the flow stress when strain softening was observed [3,17]. The data from constant load creep tests were combined with the constant velocity compression data and the results are shown in Fig.8. The flow stress, σ, and strain rate, $\dot{\epsilon}$, data for each material were fitted to the standard power law relation,

$$\dot{\epsilon} = A \, \sigma^n \qquad (2)$$

where A is a constant and n is the stress exponent. The values of A, n and the coefficient of determination, R_d^2, are listed in Table 2. The results show that all the materials are in a single deformation regime within the boundary of the current investigation showing a good linear fit

through the data collected from two different methods, constant load creep and constant compression test.

Table 2. The power law fits of the true compressive flow stress - strain rate relationship for NiAl composites at 1300K

Sample	A (sec^{-1})	n	R_d^2
NiAl-AlN	5.97×10^{-26}	9.1	0.996
NiAl-AlN-5Al$_2$O$_3$	2.88×10^{-22}	7.5	0.998
NiAl-AlN-15Al$_2$O$_3$	5.18×10^{-24}	8.0	0.997
NiAl-AlN-30Al$_2$O$_3$	3.42×10^{-24}	7.8	0.994

The flow stress-strain behavior of NiAl-5%AlN is in quite good agreement with the results previously reported for NiAl-10%AlN [3,4] except that the stress exponent of the current material (~9) is smaller than the others (>11). This difference in the stress exponent and the fact that our 5% AlN monolithic alloy is comparable with Whittenberger et al.'s 10% AlN rather than their 5% AlN are probably the result of the difference in the microstructure induced from the different processing route (MA vs. cryomilling). In particular there is a difference in the distribution of the AlN particles. Cryomilled NiAl has an inhomogeneous distribution of dispersoid , essentially located in prior particle grain boundaries, while MA NiAl has dispersoids located both at grain boundaries and in the matrix.

The composites have an average stress exponent of 7.7. As fiber vol. fraction increases the flow strength increases at all strain rates. The 5% composite is stronger than the monolithic material at high strain rates ($\geq 1 \times 10^{-4}$ s^{-1}), but it is weaker than the monolithic material at slow strain rates ($\leq 1 \times 10^{-5}$ s^{-1}) due to the smaller stress exponent. By reinforcing with 15 or 30 vol. % Al$_2$O$_3$ fibers, strengthening was achieved at all strain rates investigated.

According to the model suggested by Rösler et al.[20], the two different types of reinforcements in NiAl-AlN-Al$_2$O$_3$ composites are those of ideal size and shape for retarding creep, i.e. for improving the high temperature strength of the NiAl matrix. The high creep strength of this composite compared to non-MA monolithic NiAl results from; (1) fine AlN and Al$_2$O$_3$ dispersion particles (typically less than 1 μm), distributed homogeneously both along the grain boundaries and within the grains, which inhibit dislocation movement. This is supported by TEM studies of the NiAl matrix in the 15% composite tested at 1300K and 8.5x10^{-4} which show AlN particle-dislocation interaction, Fig.9. (2) large aspect ratio (diameter:length = 12 μm:3000 μm) fibers can improve the strength by constraining the macroscopic flow over a wide strain rate range. Such a large aspect ratio can minimize the diffusional assisted flow in composites which often causes ineffectiveness of fibers or even degradation of the matrix strength. The fiber/matrix interface in a deformed composite was also examined but no significant change was noted compared to the as-hot pressed material.

At 1300K, the NiAl-5AlN-30Al$_2$O$_3$ has more than five orders of magnitude slower creep rate than XD processed NiAl [21] and about two orders of magnitude slower creep rate than XD

processed NiAl-30%TiB$_2$ [21]. The strength of this composite approaches that of NASAIR 100 [22], a first generation Ni-base single crystal superalloy, Fig.10. Constant load creep tests are being conducted to study slow strain rate behavior (below 10^{-7}/sec) of the composites as well as monolithic material. An extensive microstructure evaluation of the composites is currently underway to identify the strengthening mechanism(s) of the composites. Further improvement in the strength of these materials is feasible through microstructure modification, such as grain coarsening through secondary recrystallization [23,24] and fiber alignment. Fibers with higher creep resistance would also produce an improvement in strength.

4. CONCLUSIONS

(1) NiAl powder containing about 5% AlN dispersion was synthesized by mechanical alloying of elemental nickel and aluminum under a nitrogen gas atmosphere.

(2) Composites containing 5, 15 and 30 vol.% of Al$_2$O$_3$ fibers in addition to the AlN dispersion particles were fabricated by hot pressing a dry blend of the MA NiAl powder and the fibers.

(3) As-fabricated microstructures revealed that the composite is fully dense and bonded well with the randomly distributed Al$_2$O$_3$ fibers. Neither chemical reaction nor cracks were observed at the fiber/matrix interface.

(4) The compressive strength was studied at 1300K at strain rates varying from 8.5x10^{-4} to 2.3x10^{-8} sec^{-1}. The stress exponent of NiAl-5AlN is 9.1 and the average stress exponent of composites is 7.7. The flow stress-strain rate behavior indicates that the creep rate of NiAl-5%AlN-30%Al$_2$O$_3$ is more than five orders of magnitude slower than XD processed NiAl and about two orders of magnitude slower than XD processed NiAl-30%TiB$_2$. The current composite is one of the strongest NiAl-based alloys along with cryomilled NiAl-30%AlN, which approaches the level of NASAIR 100, a first generation Ni-base single crystal superalloy.

5. REFERENCES

[1]   R. Darolia, *J. of Metals*, 43 (3) (1991) 44.
[2]   R.D. Noebe, R.R. Bowman and M.V. Nathal, *Int. Mater. Revs.*, 38 (1993) 193.
[3]   J.D. Whittenberger, E.Arzt and M.J. Luton, *J.Mater.Res.*, 5 (12) (1990) 2819.
[4]   J.D. Whittenberger, *Structural Intermetallics, ed. R.Darolia et.al.* (TMS, 1993) 819.
[5]   M.G.Hebsur, J.D.Whittenberger, C.E. Lowell and A.Garg, *Mat. Res.Soc.Symp.Proc.*, 364 (1995) 579.
[6]   S. Wu, *Ph.D. thesis*, (Illinois Institute of Technology, 1996).
[7]   H.Choo, P.Nash and M.Dollar, *Processing and Fabrication of Advanced Material V*, (TMS) (1996) 361.

[8]   C. Liu et al., *Materials Science and Engineering.* A191 (1995) 49.

[9]   R.D. Noebe et al., *Mat. Res.Soc.Symp.Proc.*, 194 (1990) 323.

[10]   R.R. Bowman, *Mat. Res.Soc.Symp.Proc.*, 273 (1992) 145.

[11]   P.L. Anton et.al., *Mat. Res.Soc.Symp.Proc.*, 273 (1992) 157.

[12]   R.R. Bowman et. al., *Metall. Trans. A*, 26A (3) (1995) 615.

[13]   A.K. Misra, *NASA Contractor Report 4171*, (1988).

[14]   L.R. Visser, (Ceramic Materials Department, 3M company, St. Paul, MN., 1994).

[15]   H. Ardy, *Ph.D. thesis,* (Illinois Institute of Technology, 1994).

[16]   S.J. Hwang, *Ph.D. thesis,* (Illinois Institute of Technology, 1992).

[17]   J.D. Whittenberger, *Materials Science and Engineering*, 73 (1985)87.

[18]   S.Suh, M.Dollar and P.Nash, *Materials Science and Engineering*, A192 (1995) 691.

[19]   M.Dollar, P.Nash, S.Dymek, S.J.Hwang and S.J.Suh, *Annual Report, AFOSR-90-0152B* (1992).

[20]   J.Rösler, G.Bao and A.G.Evans, *Acta Mater.* 39(11)(1991) 2733.

[21]   J.D.Whittenberger, R.K.Visvanadham, S.K.Mannan and B.Sprissler, *J. Materials Science*, 25(1990)35.

[22]   M.V. Nathal and L.J. Ebert, *Metall. Trans. A*, 16A(1985) 427.

[23]   S.C.Ur, P. Nash and G.T. Higgins, *Scripta Materiall.* 34 (1996) 53.

[24]   P. Grahle and E. Arzt, *Acta mater.* 45(1) (1997) 201.

Nickel Powder —— Aluminum Powder

Blend

Chopped Al2O3 fiber

N2 Gas —— Mechanical Alloying

Heat cleaning

MA NiAl
(NiAl- 5 vol.% AlN Dispersion)

Blend with 0,5,15 or 30 vol. % of Al2O3 Fiber

Hot Pressing @ 1473K, 120MPa, 3hours, Ar gas

Composites
MA NiAl- 0, 5, 15 or 30% Al2O3

Machining

Microstructure
Characterization

Mechanical Property
Characterization
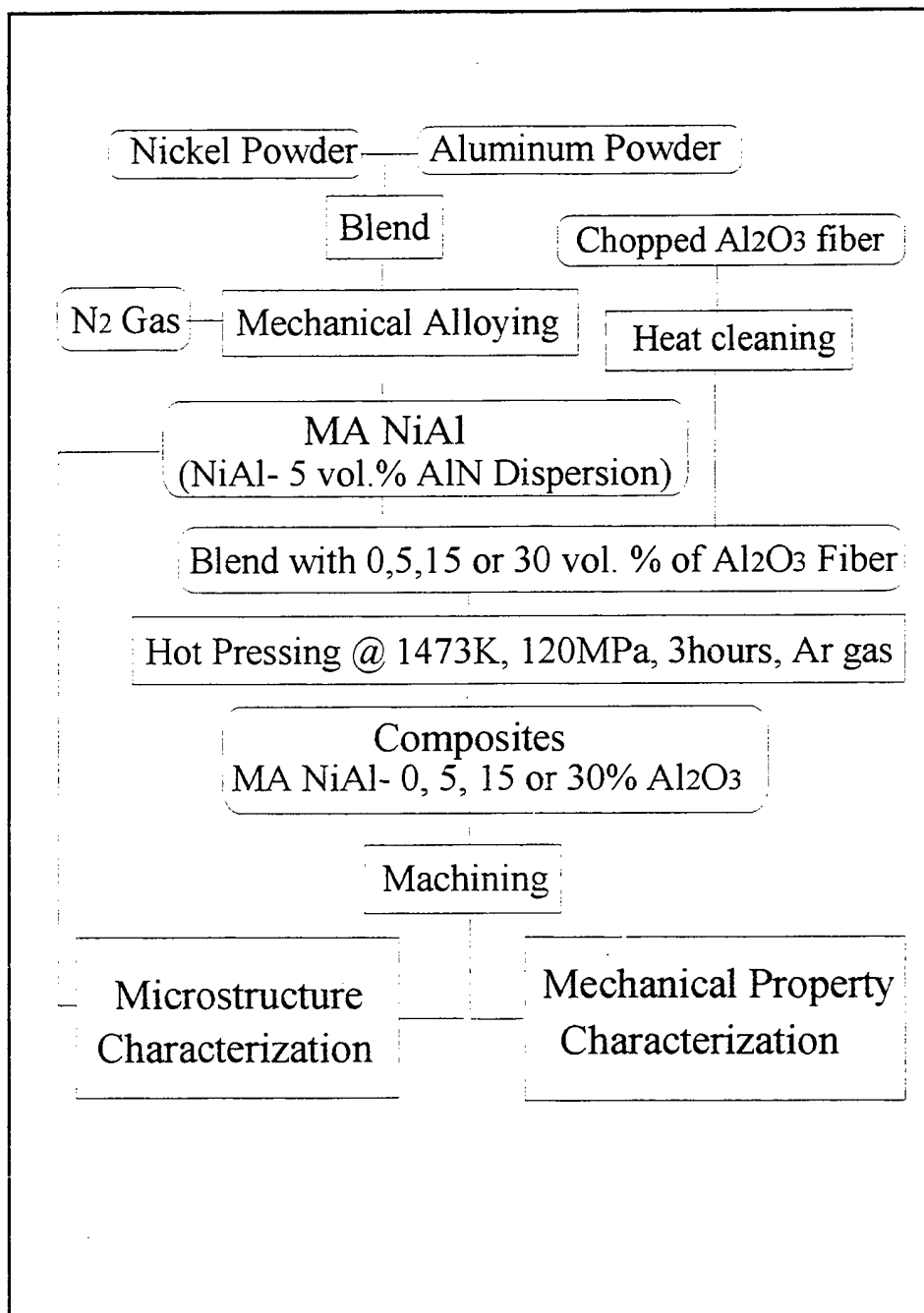
Fig. 1. NiAl-AlN-Al₂O₃ composite processing route.
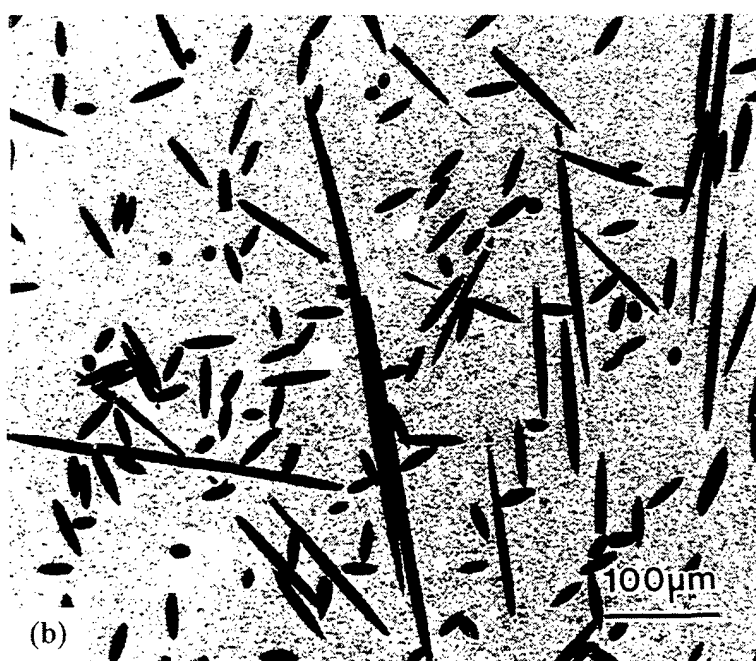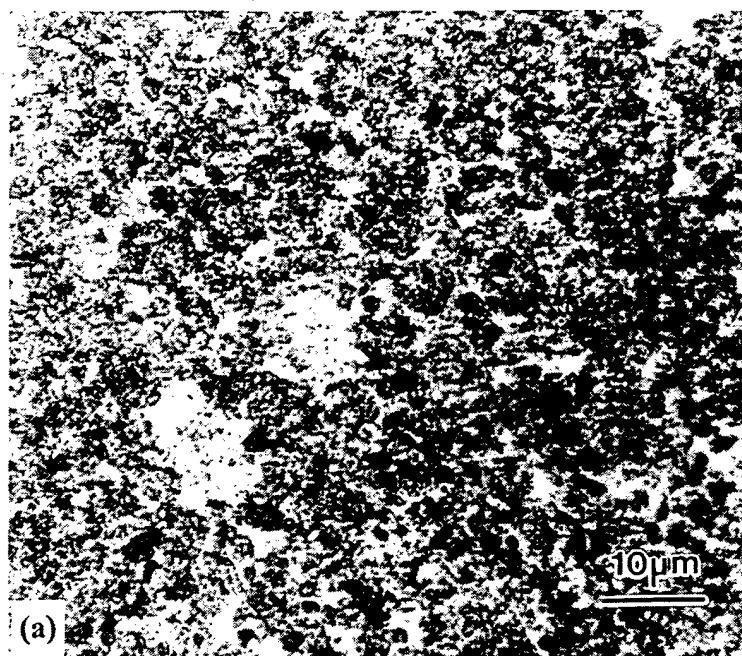
Fig. 2 Light optical micrographs of the as-hot pressed materials. (a) NiAl-5 vol.% AlN, unetched (b) NiAl-5vol.% AlN-30 vol.% Al_2O_3, unetched.

Fig. 2. Cont. Light optical micrographs of the as-hot pressed materials. (c) NiAl-5vol.% AlN-30 vol.% Al₂O₃, unetched.
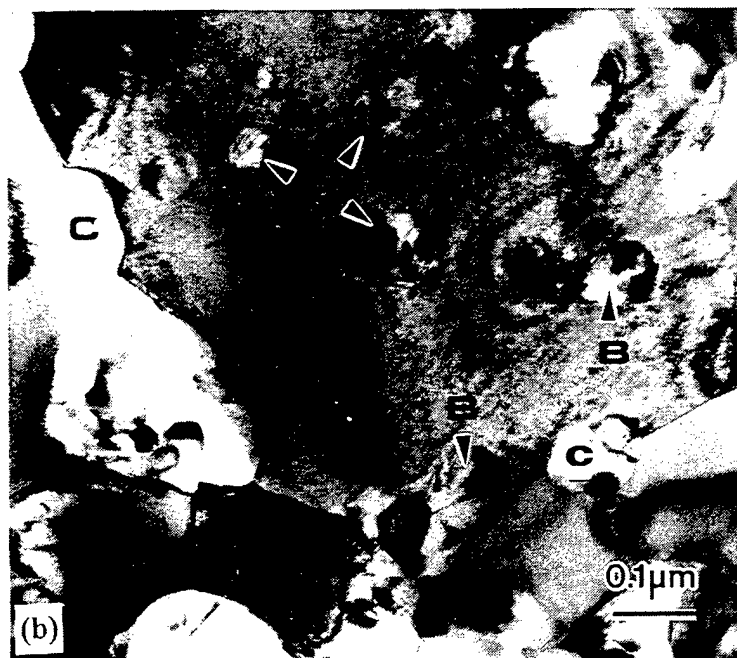
Fig. 3. TEM micrographs of the as-hot pressed NiAl-5 vol.% AlN. (a) an overview (A: NiAl matrix, ➤: dispersoid particles) (b) Dispersion particle distribution (B: AlN, C:Al₂O₃)
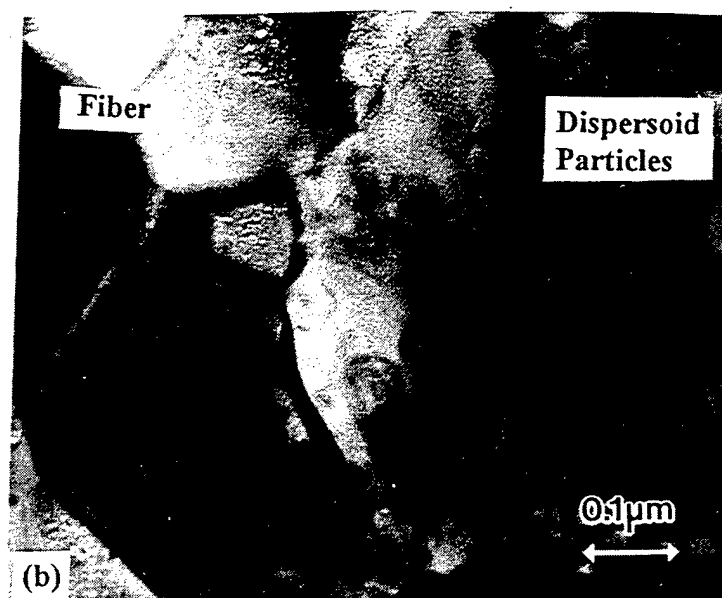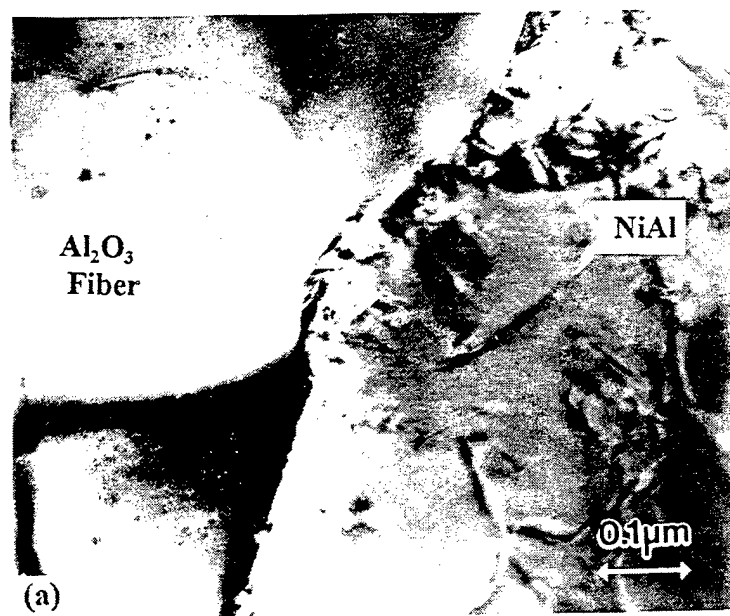
Fig. 4. TEM micrographs of the as-hot pressed NiAl-5AlN-15Al₂O₃ composite (a) interface between NiAl grain and the Al₂O₃ fiber (b) interface between dispersion particle and the Al₂O₃ fiber.
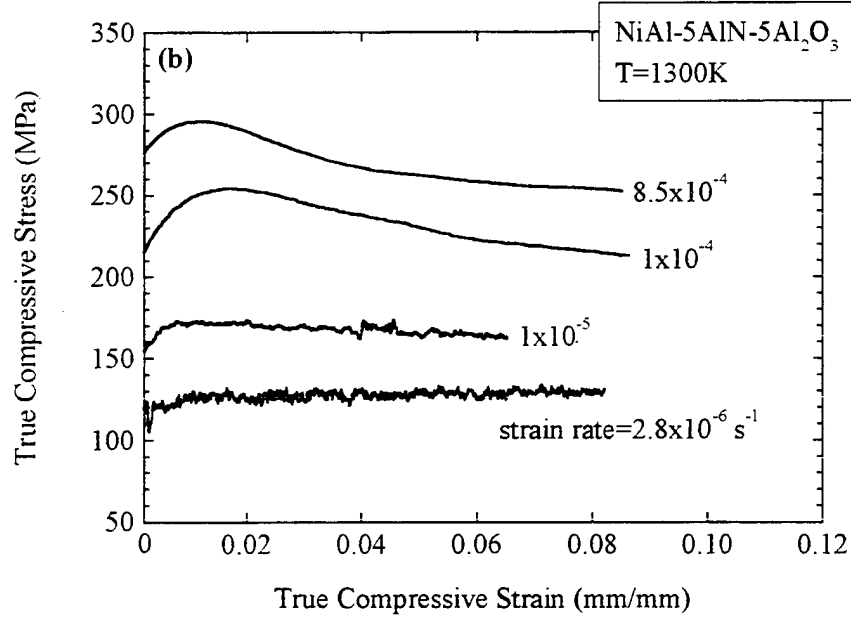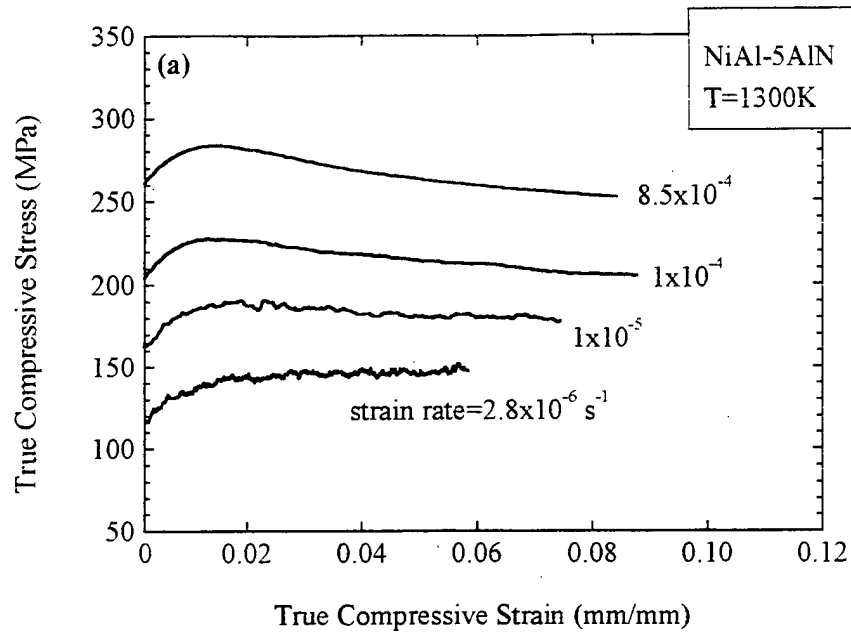
Fig. 5. True compressive stress-strain curves of NiAl-AlN-Al$_2$O$_3$ composites tested at 1300K as a function of strain rate. (a) NiAl-5AlN (b) NiAl-5AlN-5Al$_2$O$_3$.
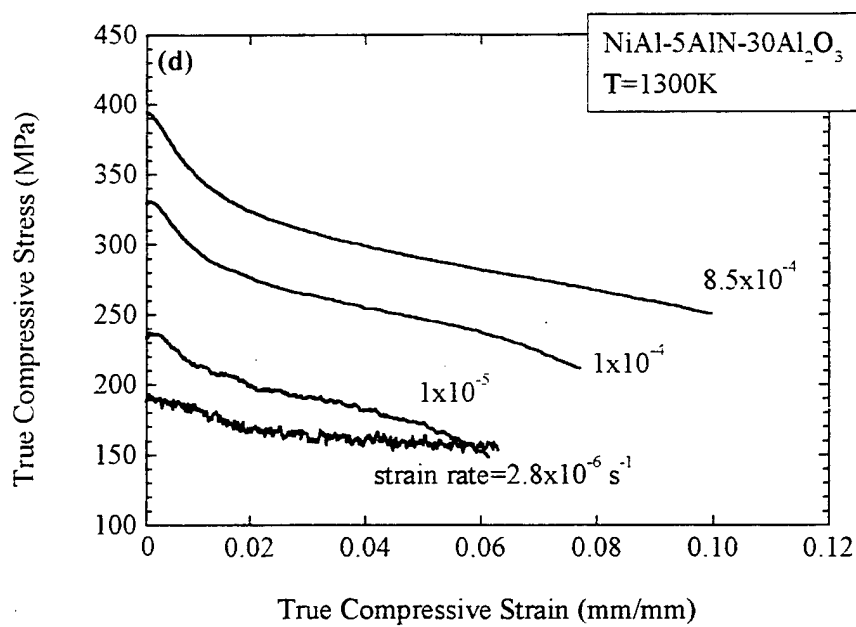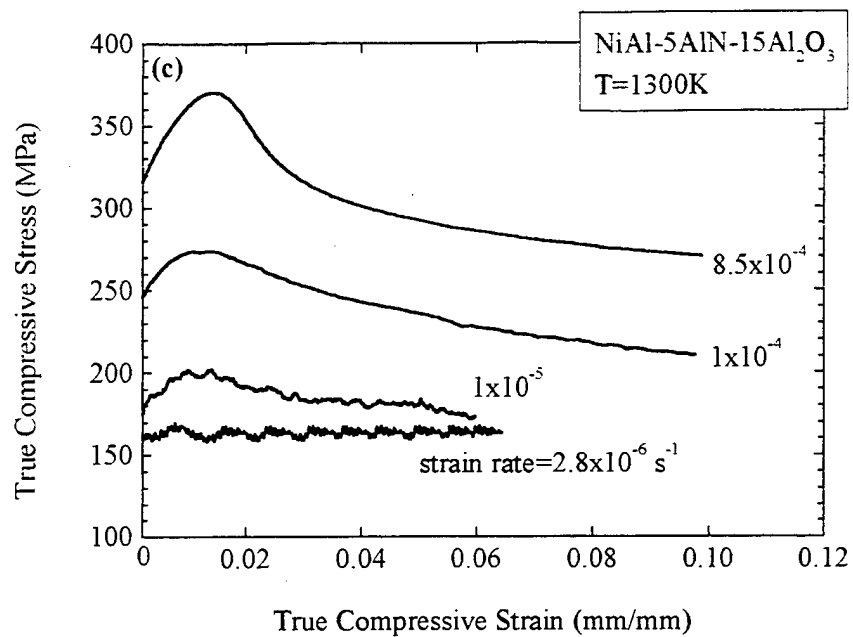
Fig. 5. Cont. True compressive stress-strain curves of NiAl-AlN-Al$_2$O$_3$ composites tested at 1300K as a function of strain rate. (c)NiAl-5AlN-15Al$_2$O$_3$ (d) NiAl-5AlN-30Al$_2$O$_3$.
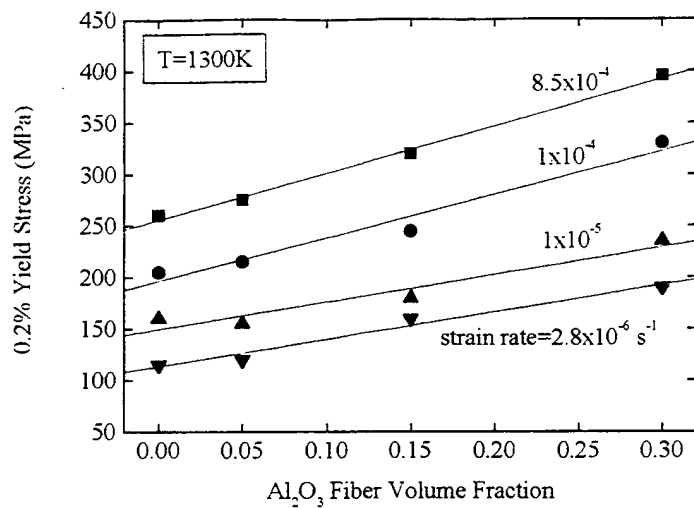
Fig. 6. 0.2% compressive yield stress of the NiAl-AlN-Al$_2$O$_3$ composites tested at 1300K as a function of Al$_2$O$_3$ fiber volume fraction at various strain rates.
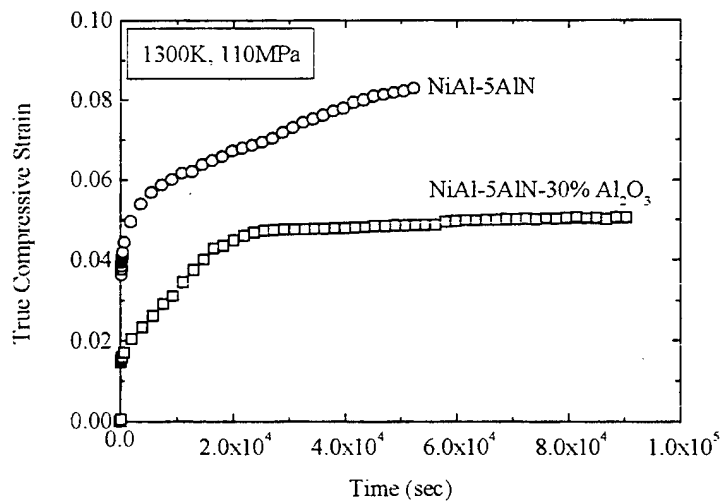

Fig. 7. Constant load compressive creep curves of NiAl-5AlN and NiAl-5AlN-30Al$_2$O$_3$ composite tested at 1300K and 110MPa.
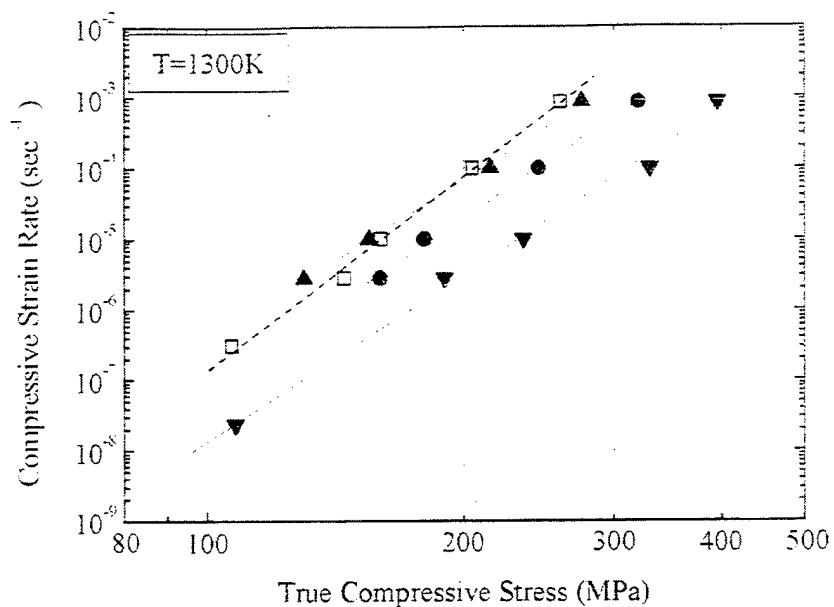
Fig. 8. True compressive stress-strain rate behavior of NiAl-AlN and NiAl-AlN-Al$_2$O$_3$ composites tested at 1300K as a function of Al$_2$O$_3$ volume fraction. (□ NiAl-AlN; ▲ NiAl-AlN-5Al$_2$O$_3$; ● NiAl-AlN-15Al$_2$O$_3$; ▼ NiAl-AlN-30Al$_2$O$_3$).
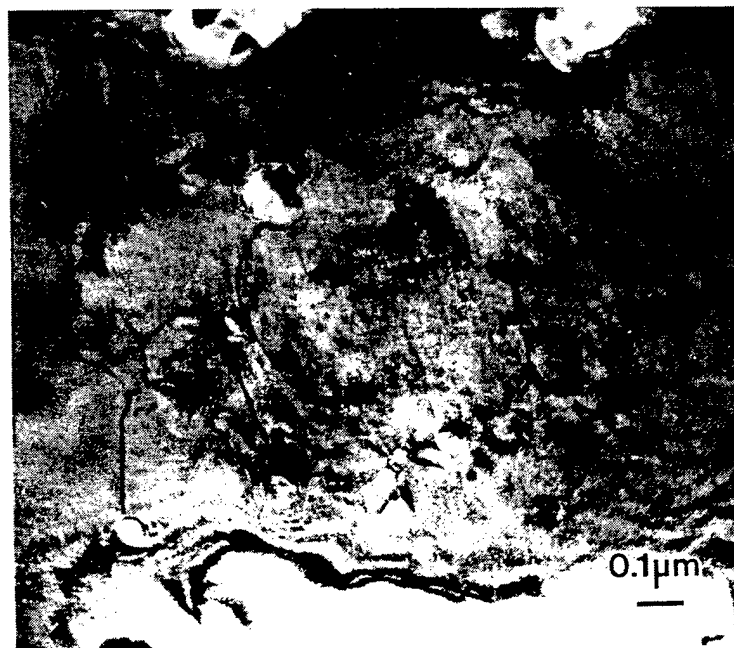

Fig. 9. TEM micrograph showing AlN particle-dislocation interaction in NiAl matrix in the 15% Al$_2$O$_3$ composite tested at 1300K and 8.5x10^{-4} s^{-1}.

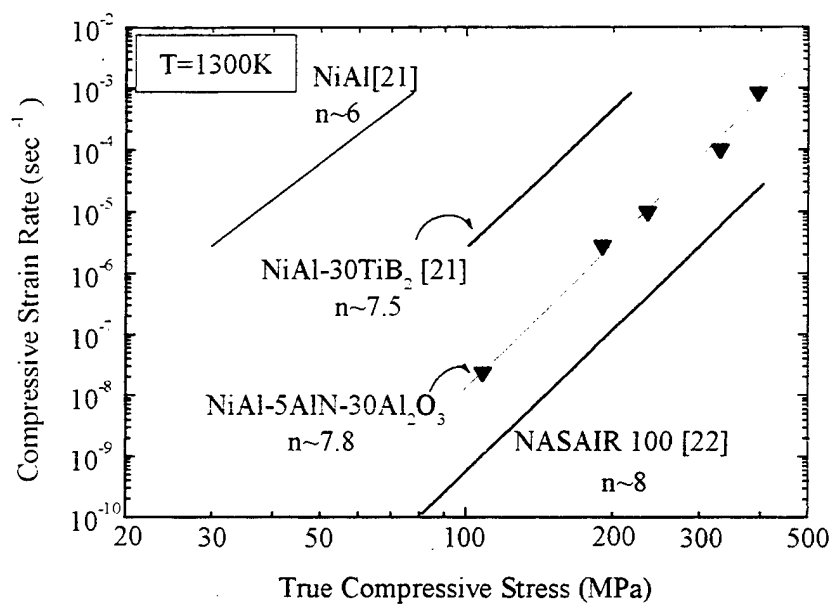Fig. 10. Comparison of the 1300K flow stress-strain rate properties of XD NiAl, XD NiAl-30%TiB$_2$, NiAl-AlN-30%Al$_2$O$_3$ and NASAIR 100.

PART C : Nb$_3$Al-BASED MATERIALS

SYNTHESIS AND CHARACTERIZATION OF MECHANICALLY ALLOYED INTERMETALLIC Nb$_3$Al-BASE ALLOYS

1. INTRODUCTION

Prior to the advent of ceramic superconductors, the Nb$_3$Al compound was extensively studied as a prime, high-temperature superconducting material. Now it is considered as a potential material for high temperature structural applications because of its high melting point (2060 C), moderate density (7.26 g cm^{-3}) and tolerance to some deviations from stoichiometry enabling its alloying. The Nb$_3$Al phase exhibits the A15 crystal structure and is extremely brittle at temperatures below 1475 K [1,2]. To date, Nb$_3$Al has had no structural use. One approach to improving the ductility and toughness of any brittle material is to incorporate a ductile phase into the brittle matrix in order to prevent crack propagation [3]. Another approach is to reduce the grain size [4]. The goal of the present study was to combine these two approaches by processing (via mechanical alloying (MA)) a fine grained Nb - Al material containing a ductile Nb solid solution and the Nb$_3$Al compound.

The paper presents results of our preliminary studies of this novel material. The investigation is an extension of our research carried out on mechanically alloyed NiAl-based intermetallics to more refractory intermetallics. Our previous studies proved that MA is a viable processing route for production of NiAl-based intermetallics [5,6] with improved mechanical properties compared to their cast counterparts.

2. MATERIAL PROCESSING

The materials investigated in this study were produced by mechanical alloying of pure elemental powders in a Szegvari-type laboratory attritor mill. The appropriate amounts of powders were mixed to give the nominal compositions: Nb - 18 at. % Al (Nb18Al) and Nb - 20 at. % Al (Nb20Al). The total milling time comprised 2 hours at about -110 C and 85 hours at room temperature (water cooling) with rotational speed of about 450 rpm. The milling was carried out in a stainless steel tank using stainless steel balls with a 3/16" diameter, in an argon atmosphere at the controlled oxygen level of 1 - 3 wt. ppm. The ball-to-powder ratio was 11:1. The powders collected at the end of milling were sieved through a 325 mesh prior to consolidation. The powder used for consolidation is shown in Fig. 1.

Consolidation was carried out by hot pressing in an argon atmosphere at 1150 C for 2 hours. The resulting material, in the form of cylinder compacts, was free from cracks with an average density of 7.8 g/cm^3 (Nb18Al) and 7.2 g/cm^3 (Nb20Al).

3. EXPERIMENTAL PROCEDURES

The consolidated material was characterized by X-Ray diffraction using CoK

radiation, scanning and transmission electron microscopies, and mechanical testing comprising hardness measurements by Vickers indenter at a 5 kG load, compression tests and creep tests.

The 10 mm high by 5 mm diameter cylindrical test specimens were electro-discharge machined from the center of the hot pressed compacts, away from the edge, to avoid regions of lower density.

Compression tests were conducted on the Nb18Al alloy at room temperature, 800 C, and 1000 C. All compression tests were carried out at a constant cross-head speed of 0.5 mm/min (strain rate   8.3 10^{-4} s^{-1}).

Compression creep tests were performed in air using a SATEC M-3 creep machine. The testing was conducted over a 24 hour period in which displacement was sampled at 3 minute intervals. The displacement was converted to strain which was plotted as a function of time. The steady-state strain rate (minimum creep rate) for each test was determined using a linear regression fit. Samples were tested under 40, 110 and 180 MPa loads at 875 C in order to determine the apparent stress exponent, n.
The activation energy for creep, Q, was determined from the Arrhenius-type plot of the temperature dependent creep rate at constant stress. This was done by testing samples at a constant stress of 110 MPa for temperatures of 875 C, 825 C and 775 C.

The disks for analytical Transmission Electron Microscopy (TEM) examinations were electropolished in a Struers Tenupol 2 jet electropolisher followed by 2 hours ion milling at low energy operating conditions (3 kV, 2 mA). TEM investigation was carried out using a Phillips CM 200 analytical transmission electron microscope operating at 200 kV equipped with an Oxford-Link X-ray Energy Dispersive Spectrometer (XEDS).

4. RESULTS

X-Ray diffraction analysis. X-Ray diffraction spectra, one of which is shown in Figure 2, were obtained from the consolidated material to identify the constituent phases. Three main phases were identified: Nb solid solution (Nb_{ss}), the Nb_3Al phase with the cubic A15 crystalline structure and a   - type Nb_2Al tetragonal phase. Also small peaks coming from Al_2O_3 were recognized. No peaks from Al were identified indicating that the entire aluminum content was tied to niobium and oxygen.

Hardness. Since microhardness measurements gave large scatter of results, regular hardness tests were carried out. At 5 kG load, the values of Vickers hardness of the Nb18Al and Nb20Al specimens were 644 and 810 HV, respectively. While indentations in the Nb18Al specimen were microcrack-free, the indentations in the Nb20Al specimen exhibited microcracks originating at indentations' corners. The much higher value of hardness for Nb20Al sample corresponds to a lower content of the Nb_{ss} phase, an observation consistent with the X-Ray analysis.

Compressive behavior. The compression properties of the Nb18Al alloy at room temperature, 800 C and 1000 C are listed in Table 1. The properties of mechanically alloyed NiAl prepared for a previous study [7,8] using the same processing and consolidation techniques are also included in Table 1. Mechanically alloyed Nb18Al showed a remarkable retention of strength superior to that in the nickel aluminides. The Nb18Al alloy exhibits almost the same compression properties at 1000 C as the NiAl at 800 C. However, at 1000 C, work softening

occurred upon reaching the maximum stress, allowing for the deformation of the specimen to near 20% strain at which value the test was stopped. Typical strain-stress curves at different temperatures for the Nb18Al alloy are shown in Fig. 3. The yield stress of the specimen decreases rapidly with increasing testing temperature. There is no indication of serrations or stress drops suggesting that uniform deformation took place in all specimens tested. The compressive strength increases with increasing aluminum content which is attributed to the corresponding decrease in the volume fraction of Nb_{ss} phase.

Creep behavior. The results of the creep tests of a Nb20Al sample conducted at 875 C are shown in Fig. 4. The steady-state creep rates determined for Nb18Al and Nb20Al at 875 C are listed in Table 2. The strain versus time curves, Figures 4 and 5, illustrate the extent of deformation endured by the specimens during the test. The amount of deformation was less for Nb20Al samples. The difference between the materials, however, becomes less pronounced at lower values of stress. The values of the steady-state creep rate for the Nb18Al samples were 1.5 to 2.3 times higher than those in Nb20Al.

Additional creep tests of Nb20Al, conducted at 110 MPa and at temperatures of 825 C and 875 C enabled the activation energy for creep to be calculated. The relevant creep curves are shown in Fig. 5. The activation energy of Nb20Al was calculated to be 371 KJ/mol, and is listed along with the minimum creep rates at 110 MPa in Table 3.

Transmission Electron Microscopy. The average grain size estimated on electron micrographs is less than 1 m (Fig. 6). The intermetallic phases can be easily distinguished from the niobium solid solution: niobium grains contain high dislocation density while in Nb_3Al as well as in Nb_2Al numerous stacking faults occur (Fig. 6). Small Al_2O_3 particles embedded in other phases or appearing on grain boundaries have rounded shapes, though bigger oxides - on the order of grain size - were also found.

Stacking faults were found in the Nb_3Al phase of the as-received material (Figs 7, 8) and even more in the deformed specimens. These defects lie predominantly on {100} planes. Some partial dislocations had <100>-type Burgers vector, however, in many cases, Burgers vectors, and consequently, the displacement vector for these faults, have not been determined. The stacking faults exhibited rather complex behavior giving sometimes nonsymmetric fringe contrast. The termination of these faults on grain boundaries (Fig. 8) or on other larger faults rather than on partial dislocations was often observed. No perfect dislocations were found. The stacking faults in the Nb_2Al phase exhibit even more complex character and have not been analyzed yet.

5. DISCUSSION

The presence of the solid solution Nb_{ss} and Nb_3Al was predicted based on the analysis of the Nb-Al phase diagram, the dispersoids are a natural product of mechanical alloying whereas the occurrence of the unexpected tetragonal phase can be rationalized by the nature of mechanical alloying that frequently produces far-from-equilibrium phases as a result of large amounts of impurities shifting phase boundaries on the respective phase diagrams. Also, an incomplete homogenization during consolidation may contribute to the presence of that non-equilibrium phase. The high density of dislocations in Nb_{ss} grains, observed in both as-received

and deformed specimens, can be explained by a significant difference in the coefficient of thermal expansion between the intermetallic and Nb_{ss} phases [9].

The A15 crystal structure of the Nb_3Al compound can be depicted as a b.c.c. lattice formed by Al atoms and orthogonal chains of Nb atoms, parallel to the <100> directions, crisscrossing the b.c.c. arrangement of Al atoms. Such structure can be also described in terms of the stacking of three different types of layers, *a b a b*, parallel to the cube faces - Fig. 9 [10, 11]. Each layer corresponds to {400} planes in the structure. Removing one or more *a* or *b* closely packed layers produces stacking faults in such a structure. None of the layers has the stoichiometric composition and thus the removal of a layer to produce a stacking fault will cause a local change in composition.

The presence of such stacking faults may play a role in "absorbing deviations from stoichiometry" [10]. Attempts to find a correlation between the presence of stacking faults and a deviation from stoichiometry support partly this hypothesis. The aluminum content in grains containing stacking faults measured by XEDS, changed from ca. 14% to 28% at. but the most common concentration was 16-18%. Some grains without any stacking faults exhibited much smaller deviation from stoichiometry (Al content was always above 20% at.). It is interesting to note that some grain compositions correspond to phases Nb_5Al (17 at. % Al) and Nb_5Al_2 (29 at. % Al) that were reported in the Nb-Al system by Richards [12,13], however, never confirmed later. As far as stoichiometric composition is concerned, the hypothetical Nb_5Al phase corresponds to the stacking fault formed by removing the plane **a**, and the Nb_5Al_2 "phase" may occur as a result of removing the plane (Fig. 9). The composition that matches the latter phase was found only occasionally suggesting that this kind of stacking fault is less common in the Nb_3Al structure. Fig. 10 shows several grains with different concentration of Al (at. %): A - 23% (Nb_3Al), B - 17%, C - Al_2O_3, D - 4% (Nb_{ss}). Selected area diffraction patterns (SADPs) taken from grains exhibiting large deviation from stoichiometry (grain B in Fig. 10) do not correspond to a cubic phase while those with small deviations (grain A in Fig. 10) strictly match the Nb_3Al phase. One can also speculate that such phases may appear as metastable phases which decompose later to a mixture of Nb_{ss}, Nb_2Al and Nb_3Al phases. Though the number of such grains is not significant (below detection by X-Ray spectroscopy), further investigation utilizing convergent beam electron diffraction may help to find out if the grains constitute really separate phases or are just off-stoichiometric grains of the Nb_3Al phase.

The appearance of stacking faults in Nb_3Al strictly corresponds to the situation described earlier by Smith et al. [10] and their hypothesis regarding the origin of stacking faults formed as a result of the coalescence of point defects is supported by the present TEM studies. However, the fact that more stacking faults were found in the deformed specimen suggests that they may have been produced by glide processes. Indeed, Murayama et al. [9] have recently reported that high densities of planar faults bounded by partial dislocations are formed on {100} planes during plastic deformation above 1473 K. Murayama et al. [9] found the Burgers vector of the partial dislocations and the displacement vector of the stacking fault to be <100>. In our study, the Burgers vector of partial dislocations, <100>, was also determined. This leads us to hypothesize that <100>{001} slip controls plastic deformation and the hypothesis rationalizes the Nb_3Al brittleness.

The analysis of mechanical properties (compression and hardness tests) indicates that our attempt to ductilize the Nb-Al alloys by introducing the ductile Nb_{ss} phase was not fully successful since the examined samples exhibited only limited compression ductility. However, the lack of cracks on the surface of the hardness-tested Nb18Al sample may indicate that the

Al composition at which brittle-ductile transition occurs is higher than that found by Suyama et al. (16% Al) for the Nb-Al alloys [14]. This can be attributed to grain refinement in the examined alloys. Also, extensive deformation of samples tested at 1000 C suggests that the brittle to ductile transition temperature is lower in the present material than the value reported by Shah and Anton for arc-melted Nb_3Al [2].

The lower minimum creep rate of Nb20Al compared to Nb18Al is apparently due to the lower amount of the Nb_{ss} phase in the microstructure of Nb20Al. Creep properties of Nb20Al along with those of the NiAl [15] and a cast (arc melted) alloy Nb-18 at. % Al reported by Anton and Shah [16] are shown in Table 4. As it can be seen, the minimum creep rate of the Nb20Al niobium aluminide is lower than that of the nickel aluminide. The stress exponents of the two mechanically alloyed materials are almost identical. Because the two materials were synthesized by the same procedure, tested under nearly the same conditions and are both oxide dispersion strengthened, it can be assumed that the creep mechanism is the same. Traditional creep theories for simple metals predict stress exponents within the range 3 - 5 and our results also fall into this range. From our research conducted on mechanically alloyed NiAl-based alloys, it was concluded that the creep mechanism for those materials was dislocation creep in which the movements of the dislocations in the matrix were restricted by the oxide dispersoids [8]. In overcoming the obstacles, dislocations climb. Therefore, the dislocation creep of MA NiAl is ultimately controlled by vacancy diffusion. The determined value of the activation energy of MA NiAl corresponded to the range of activation energies for diffusion determined experimentally [17].

For Nb_3Al, Anton and Shah [16] modeled the activation energy for self diffusion using the inter-diffusion coefficient $= D_AN_B + D_BN_A$, where is the inter-diffusion coefficient, D_i the diffusivity of species i in the compound and N_i the molar fraction of species i. The value of the inter-diffusion coefficient for Nb_3Al was determined to be 366 KJ/mol [16]. This value closely matches the activation energy for creep of Nb20Al, 371 KJ/mol, determined in the present study.

The nearly identical values of stress exponents in Nb20Al and NiAl indicate that in the two materials the same creep mechanisms occur. These stress exponents are typical for dislocation creep, and are higher than those expected for diffusional flow. In addition, diffusional flow is believed to be predominant at temperatures greater than $0.7T_m$, higher than the present test temperatures for both NiAl and Nb20Al. The activation energy of cast Nb-18%Al [16] is comparable to that of Nb20Al and is also close to the chemical diffusion coefficient for Nb_3Al. The reported creep mechanism for the cast material is diffusion controlled dislocation climb [16]. The stress exponent for the cast material was slightly lower than that found for NiAl and Nb20Al. The lower value of the stress exponent may be attributed to the test temperature of 1200 C being near the regime for diffusional creep.

6. SUMMARY AND CONCLUSIONS

It has been shown that mechanical alloying followed by hot pressing is a viable processing route for niobium aluminide intermetallics. X-Ray spectroscopy as well as transmission electron microscopy studies revealed a multi-phase microstructure consisting of A15 Nb_3Al, b.c.c. niobium solid solution, tetragonal Nb_2Al and randomly dispersed particles of Al_2O_3. Grain sizes of constituent phases were less than 1 μm. The grains of the Nb solid solution exhibited a high dislocation density, whereas stacking faults were present in both the A15 and   phases. The improvement in strength of the mechanically alloyed material was due to the refined grain size and

oxide dispersion in the microstructure. Although they lacked room temperature ductility, their ductile to brittle transition temperature was lower than that reported for arc melted Nb-18Al. The compressive strength of the examined materials was found to be superior to the NiAl alloy processed and tested at the same conditions, but the ductility was lower. The minimum creep rates of both tested materials were found to be approximately one order of magnitude less than those in MA NiAl. The mechanism for creep deformation in mechanically alloyed niobium aluminides is postulated to be dislocation creep through diffusion controlled climb. The above findings allow me to state that the new materials exhibit potential for high temperature structural applications such as aircraft turbine blades, disks, vanes, etc. The progress in this area - the development of next generation aircraft turbine engines, hinges actually on the design and development of new, advanced, structural materials such as niobium aluminides, the materials in question.

7. REFERENCES

[1]   Y. Umakoshi, *Bull. Japan Inst. Metals*, 30 (1991) 72.
[2]   D.M. Shah and D.L. Anton, *Mat. Sci. Eng.*, A153 (1992) 402.
[3]   M.F. Ashby, F.J. Blunt and M. Bannister, *Acta Met.*, 37 (1989) 1847.
[4]   E.M. Schulson and D.R. Barker, *Scripta Met.*, 17 (1983) 519.
[5]   S. Dymek, M. Dollar, P. Nash and S.J. Hwang, *Mat. Sci. Eng.*, 152A (1992) 160.
[6]   M. Dollar, S. Dymek, P. Nash and S.J. Hwang, *Metall. Trans.*, 24A (1993) 1993.
[7]   S.J. Hwang, Ph. D. Thesis, Illinois Institute of Technology, Chicago 1992.
[8]   S.J. Suh, Ph. D. Thesis, Illinois Institute of Technology, Chicago 1994.
[9]   Y. Murayama, T. Kumagai and S. Hanada, *Mat. Res. Soc. Symp. Proc.* vol. 288, ed. I. Baker, R. Darolia, J.D. Whittenberger and M.H. Yoo, MRS (1993), p. 95.
[10]   L.S. Smith, T-T. Cheng and M. Aindow, *Mat. Res. Symp. Proc.*, vol. 288, MRS 1993, p. 263.
[11]   F. Reynaud and A.B. Lamine, Acta Met. 29 (1981) 1485.
[12]   M.J. Richards, *Memories Scientifiques Rev. Metallurg.*, 61 (1964) 265.
[13]   R.P. Elliot and F.A. Shunk, Bulletin of Alloy Phase Diagrams vol. 2. No. 1. (1981).
[14]   R. Suyama, M. Kimura and K. Hashimoto, *"Structural Intermetallics"*, ed. R. Darolia, J.J. Lewandowski, C.T. Liu, P.L. Martin, D.B. Miracle and M.V. Nathal, The Minerals, Metals & Materials Society, 1993, p. 681.
[15]   S. Suh, M. Dollar and P. Nash, *Mat. Sci. Eng.*, 192A (1995) 691.
[16]   D.L. Anton and D.M. Shah, *Mat. Res. Symp. Proc.*, vol. 133, MRS 1989, p. 361.
[17]   J.E. Dorn, *"Creep and Fracture of Metals at High Temperatures"*, National Physical Laboratory, London U.K. (1956).

Table 1. Comparison of compression properties of Nb18Al alloy and MA NiAl.

Material	Yield Strength [MPa]			Max. Strength [MPa]			Max. Strain [%]		
	R.T.	800 C	1000 C	R.T.	800 C	1000 C	R.T.	800 C	1000 C
Nb18Al	1615	884	310	2115	1344	500	1	3.2	19*
NiAl	1100	310	57	1836	325	90	2.8	17*	12*

*Strain at which test was stopped.

Table 2. The minimum creep rates [s-1] of Nb20Al at 875°C

Stress [MPa]	Nb18Al	Nb20Al
40	2.15×10^{-9}	1.34×10^{-9}
110	9.41×10^{-8}	6.92×10^{-8}
180	5.73×10^{-7}	2.56×10^{-7}
Stress Exponent	3.7	3.6

Table 3. The minimum creep rates of Nb20Al at 110 MPa

Temperature [C]	Creep Rate [s^{-1}]
875	6.92×10^{-8}
825	2.5×10^{-8}
775	1.73×10^{-9}
Activation Energy	371 kJ/mol

Table 4. Comparison of creep properties of Nb20Al, MA NiAl [15] and arc-melted Nb-18%Al [16]

Material	Min. Creep Rate [s^{-1}]	Stress Exponent	Activation Energy [KJ/mol]
Nb20Al (875 C, 110MPa)	6.92×10^{-8}	3.6	371
NiAl (850 C, 110MPa)	2.7×10^{-7}	3.5	204
Cast Nb-18%Al* (1200 C, 100MPa)	1.5×10^{-6}	2.19	347

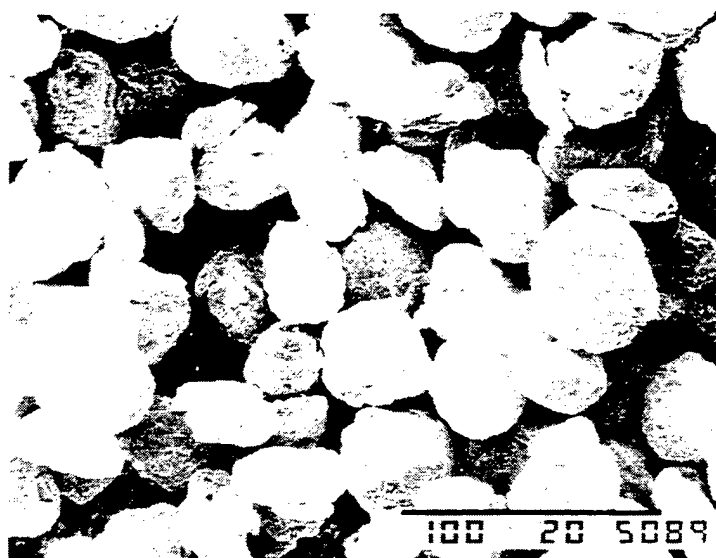* Cast Nb-18%Al samples were tested in compression under vacuum conditions [16]

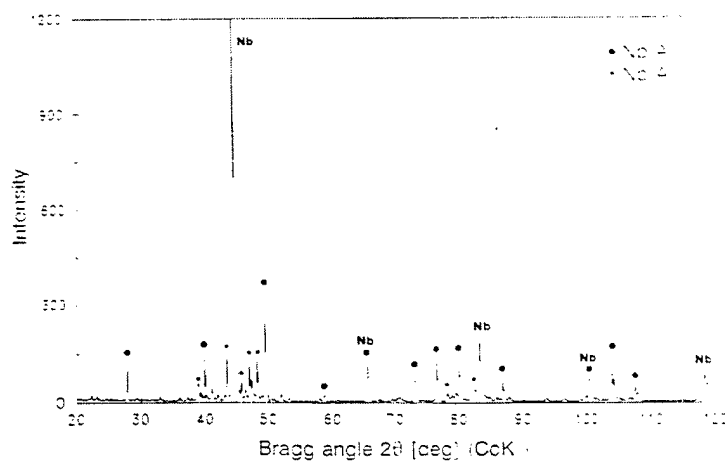Fig.1 Scanning Electron Micrograph of as-milled powder.

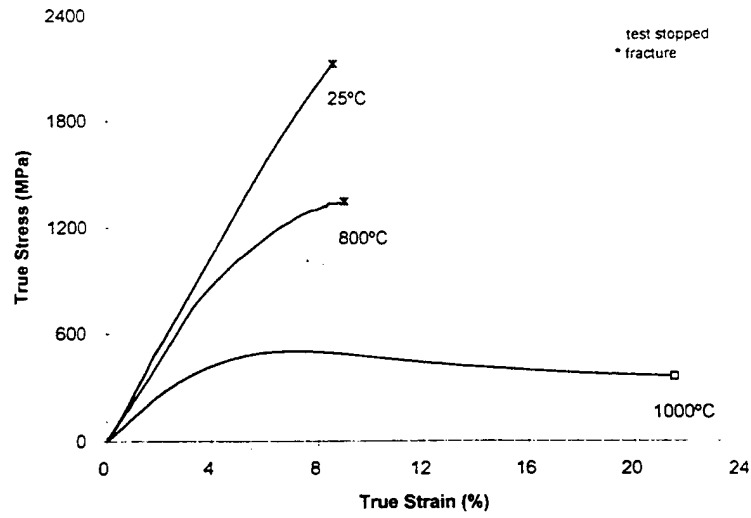Fig.2 X-Ray diffraction pattern of the Nb18Al sample.

2400

1800

True Stress (MPa)

1200

600

0

25°C

800°C

1000°C

test stopped
* fracture

True Strain (%)

Fig.3 Mechanical properties of the Nb18Al sample tested in compression.

6

4

Strain (%)

2

0

180 MPa

110 MPa

40 MPa

Time (Hr)
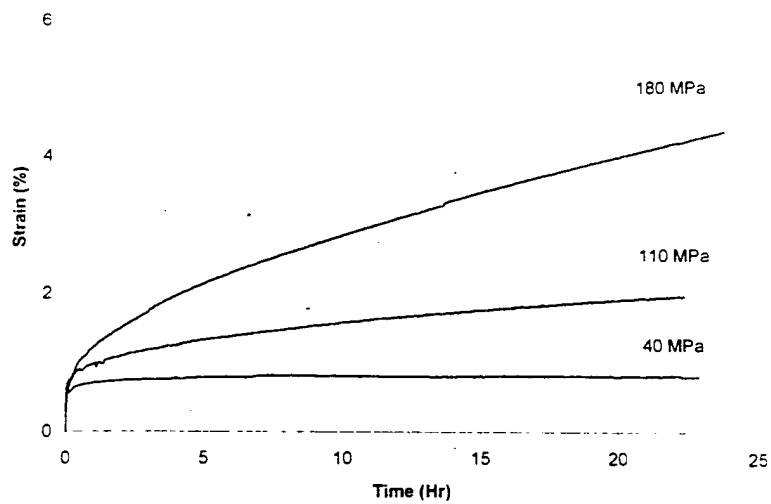
Fig.4 Creep curves of the Nb20Al sample at 875 C.
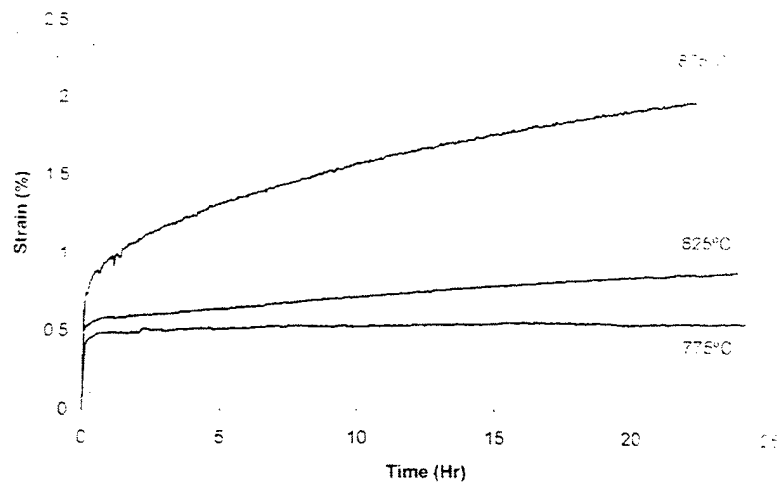
Fig.5 Creep curves for the Nb20Al sample at 110 MPa.

Fig.6 Typical microstructure of the as-hot-pressed Nb18Al sample: TEM.
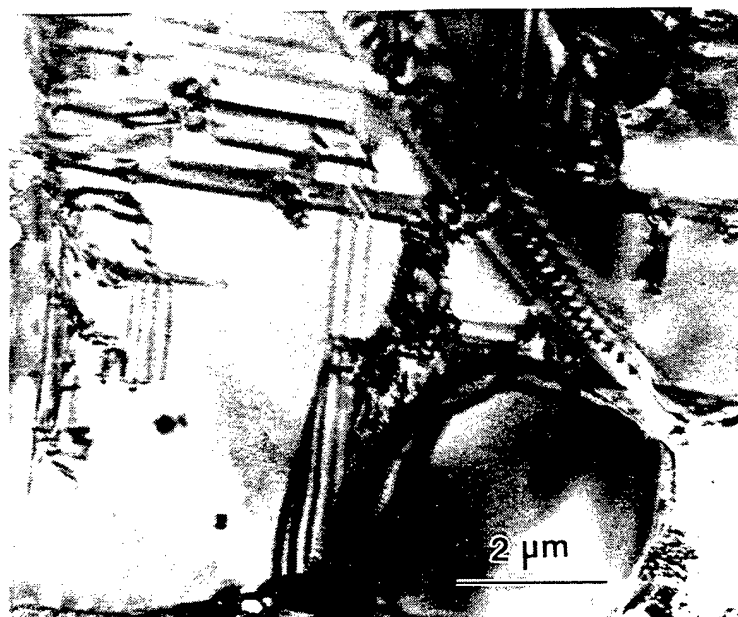
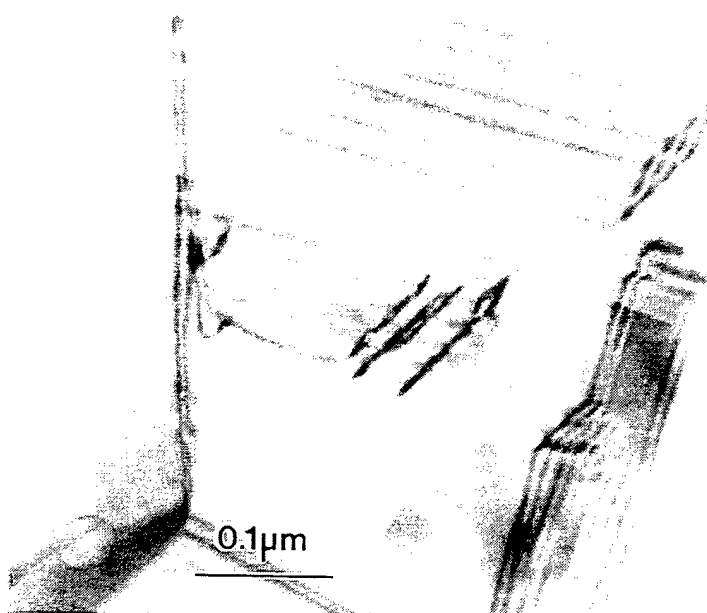Fig.7 Characteristic stacking faults in the Nb₃Al phase.

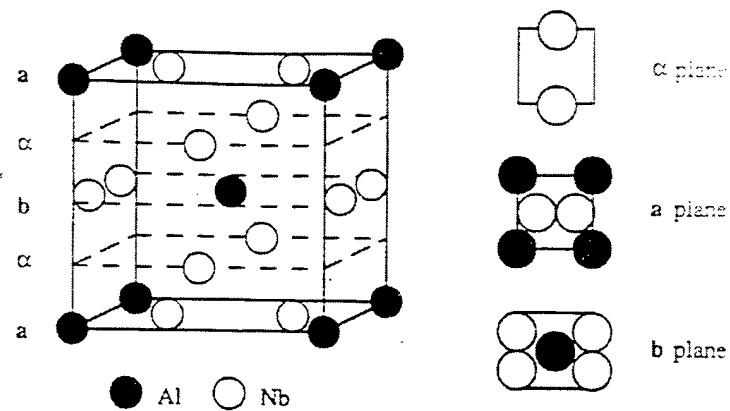Fig.8 Stacking faults in the Nb₃Al phase terminated on a grain boundary.
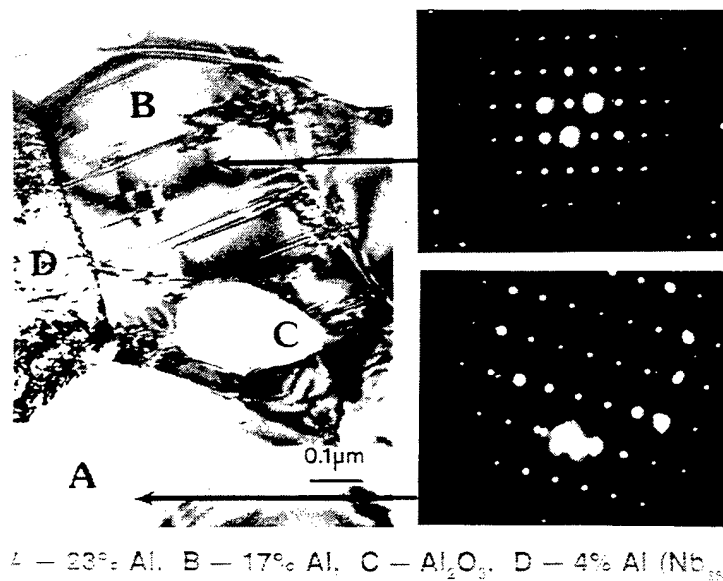
Fig.9 Arrangement of atoms in the A15 crystal structure (after Ref. [10, 11]).

A — 23% Al. B — 17% Al. C — Al₂O₃. D — 4% Al (Nbₛₛ)

Fig.10 The microstructure of the Nb18Al alloy with corresponding SADPs (SADPs not oriented with the

image). A - Nb₃Al, orientation B=[011]; B - non-cubic phase; C - Al₂O₃; D - Nbₛₛ.